Stochastic Model of Heterogeneity in Earthquake Slip Spatial distributions

Daniel Lavallée[1], Pengcheng Liu[1], and Ralph J. Archuleta[1,2]

1 Institute for Crustal Studies, University of California, Santa Barbara, California, USA

2 Department of Geology, University of California, Santa Barbara, California, USA

Accepted …….. Received ……..: in original form ……..

Abbreviated title: Stochastic model of slip

Corresponding author: Daniel Lavallée. Institute for Crustal Studies, University of California, Santa Barbara, CA 93106, USA. Tel: 805-893-8446; Fax: 805-893-8649; Email: daniel@crustal.ucsb.edu

P. L: pcliu@crustal.ucsb.edu

R. J. A: ralph@crustal.ucsb.edu

Paper submitted in November 2004 for publication in Geophysical Journal International. Further reproduction or electronic distribution is not permitted.

Summary: Finite-fault source inversions reveal the spatial complexity of earthquake slip or pre-stress distribution over the fault surface. The basic assumption of this study is that a stochastic model can reproduce the variability in amplitude and the long-range correlation of the spatial slip distribution. In this paper, we compute the stochastic model for the source models of four earthquakes: the 1979 Imperial Valley, the 1989 Loma Prieta, the 1994 Northridge and 1995 Hyogo-ken Nanbu (Kobe). For each earthquake (except Imperial Valley), we consider both the dip and strike slip distributions. In each case, we use a one-dimensional stochastic model. For the four earthquakes, we show that the average power-spectra of the raw, i.e., non-interpolated, data follow a power law behavior with scaling exponents that range from 0.78 to 1.71. For the four earthquakes, we have found that non-Gaussian probability law, i.e., the Lévy law, is better suited to reproduce the main features of the spatial variability embedded in the slip distribution, including the presence and frequency of large fluctuations. Since asperity are usually defined as regions with large slip values on the fault, the stochastic model will allow predicting and modeling the spatial distribution of the asperities over the fault surface. The values of the Lévy parameters differ from one earthquake to the other. Assuming an isotropic spatial distribution of heterogeneity for the dip and the strike slip of he Northridge earthquake, we also compute a two-dimensional stochastic model. The main conclusions reached in the one-dimensional analysis remain appropriate for the two-dimensional model. The results obtained for the four earthquakes suggest that some features of the slip spatial complexity are universal and can be modeled accordingly. If this is proven correct, this will imply that the spatial variability and the long-range correlation of the slip or pre-stress spatial distribution can be described with the help of five parameters: a scaling exponent controlling the spatial correlation and the four parameters of the Lévy distribution constraining the spatial variability.

Key words: Fault slip, Inhomogeneous media, Statistical methods, Stress distribution

I INTRODUCTION

The source of complexity in earthquakes is not well understood and still debated (Carlson and Langer, 1989; Rice, 1993; and Madariaga and Cochard, 1994). Like other complex systems observed in nature, the expectation that the complexity of earthquakes may be due to some underlying scaling law comes from observations. The foremost observation in seismology is the Gutenberg-Richter statistics for the number and magnitude (energy release) of earthquakes (Gutenberg and Richter, 1942). Taken globally or locally, the logarithm of the number of earthquakes is related to the magnitude through a power law over 18 orders of magnitude in the size of an earthquake. A less well known, but critical, observation is the roughness of topography of sliding surfaces (Figure 4 in Power et al., 1987). Their basic result shows that over 11 orders of magnitude in fault surface wavelength—that is from field data to the laboratory—the power spectrum density of roughness (geometrical complexity) appears to follow a power law. This suggests that asperities and barrier are distributed —over a large range of scale— on the fault surface.

Following early observations of complexity in earthquakes (Wyss and Brune, 1967; Das and Aki, 1977; Aki, 1979; Day, 1982; and Boatwright, 1984), the complex behavior of earthquakes has been reported in almost every article based on inverting near-source data for the slip or pre-stress distribution of the causative fault (e.g. Hartzell and Heaton, 1986; Beroza and Spudich, 1988; Bouchon, 1997; and Bouchon *et al.*, 1998a, b; Sekiguchi *et al.*, 2000; Zeng and Chen, 2001; Mikumo *et al.*, 2003; and Zhang *et al.*, 2003). In a study of spatial heterogeneity and friction in the crust, Rivera and Kanamori (2002) conclude that "heterogeneity of stress field, and friction in the crust seems to be the essential feature of the crust, and studies on earthquake rupture dynamics must take these heterogeneities into consideration." As elsewhere in physical sciences, efforts to understand complex spatial variability were based on a statistical characterization approach (Boore and Joyner, 1978; Andrews 1980; Von Seggern, 1981; Lomnitz-Adler and Lemus-Diaz, 1989; Gusev 1992; Herrero and Bernard, 1994; and Oglesby and Day, 2003). Most of the models discussed in the literature are either phenomenological in nature or simply a guess. While these

models may reproduce some qualitative features of the "heterogeneous" variability observed in slip or pre-stress distribution, the model parameters are neither fixed nor validated through a comparison with the inverted slip data. Somerville *et al*., (1999) and Mai and Beroza (2002) went a step further. Using available source models, they validated and computed the parameters of the Von Karman function that they used to model the two-points statistics of the slip distributions. Guatteri *et al*. (2003), computed kinematic, hybrid and dynamic scenarios of ruptures based on synthetic random pre-stress spatial distribution modeled according to Mai and Beroza (2002). A major finding of this study was that the inclusion of variability in the source parameters is fundamental to simulate realistic ground motion time histories. In a paper discussing the dynamic inversion and modeling of the 1992 Landers earthquake, Peyrat *et al*. (2001) concluded that rupture propagation is "critically determined" by the pre-stress spatial distribution. These results suggest the importance of a proper quantification of the statistical properties associated to earthquake source models. Such quantification should go beyond "trial and error" random modeling of the slip and pre-stress spatial heterogeneity.

In a search for a better model describing the spatial distribution of heterogeneity over the fault surface, one has to find a model which includes and preserves as many features of the random or stochastic nature observed in the source models as possible. Gusev (1992) outlined the procedure to achieve this goal. In principle the random model will include one point-statistics (probability law governing the distribution of the random variables), two-point statistics (correlation function or spectrum), three-point statistics and so on. Lavallée and Archuleta (2003) introduced a random model of slip distribution validated and parameterized by computing the one point-statistics and two-point statistics associated to the Imperial Valley source model. For this reason, the results presented in this paper depart significantly from previous studies in several aspects. First, the analysis is performed on non-interpolated data,; the effect of interpolation can be profound. Second, the probability law of the random variables associated with the slip is non-Gaussian; it is a Lévy law. As shown in this paper, the usually assumed Gaussian law fails to mimic the basic result found from the data: namely a Gaussian law does not reproduce the degree of spatial variation in slip

amplitude observed on the fault. As such, a Gaussian law leads to less heterogeneity in the slip and the resulting ground motion. (The differences between the two scenarios are more obvious when watching the movie of the progression of the rupture —the movie is available at http://www.crustal.ucsb.edu/~ralph/rupture/.)

Empirical observations of non-Gaussian law of the Lévy type have been reported in seismology. For instance, analyses of the statistical properties of strong ground motion recorded in the epicentral areas of large earthquakes demonstrate that the distribution of peak acceleration is non-Gaussian (Gusev, 1996). The probability distribution is characterized by a "heavy tail" (a typical signature of Lévy distribution) and is better approximated by a Cauchy distribution (a special case of the Lévy distribution) (Tumarkin and Archuleta, 1997). These results suggest that observation of non-Gaussian distribution in the strong ground motion could have its origin in the spatial variability of the slip over the fault surface or vice-versa. Furthermore, Kagan (1994) and Marsan (2004) have shown that the stress increments caused by a fractal set of earthquakes on subsequent earthquakes is also distributed according to a Lévy law.

In this paper, we derive the stochastic model for the source models of four earthquakes: the 1979 Imperial Valley, the 1989 Loma Prieta, the 1994 Northridge and 1995 Hyogo-ken Nanbu (Kobe). For each inversion model (except Imperial Valley), we consider both the dip and strike slip distribution. In each case, we use a one-dimensional stochastic model. This choice is not the result of any particular insight or theoretical motivation but is based on pragmatic considerations. Usually source models have a larger spatial extension along the strike direction than along the dip direction. Thus the numbers of events is then larger in the former case, often constraining the statistical analysis to layers along this direction. Fortunately, the Northridge inversion is a welcome exception to this rule, and for this purpose, it is also analyzed but assuming a two-dimensional stochastic model. Finally in the appendix, we discuss the procedure adopted in this study, to compute the parameters of the Lévy law.

II STOCHASTIC MODEL OF EARTHQUAKE SLIP SPATIAL DISTRIBUTION: OVERVIEW

In Lavallée and Archuleta (2003), we proposed and tested a model that includes one-point and two-point statistics for the slip distribution of 1979 Imperial Valley earthquake. The stochastic model is similar to the fractional Brownian motion (fBm) —see Peitgen and Saupe, 1988; and Falconer, 1990. One of the procedure used to obtain fBm, consists in generating white noise distributed according to a Gaussian law over a grid or lattice (of any number of dimensions), and then to filter the noise in the Fourier space to generate a "stochastic or random process" characterized by a spectrum with a power law behavior. In Lavallée and Archuleta (2003), we relaxed the constraint that the random variables had to be distributed according to a Gaussian law and assumed the most general case of the Lévy, or stable law, (Feller, 1971; Grigoriu, 1995; Nikias and Shao, 1995; and Uchaikin and Zolotarev, 1999). The underlying idea in adopting this generalization of fBm is that the probability laws as well as the PDF parameters characterizing the stochastic model are both fixed by the data. As we will see in the next sections, assuming that the one-point statistics are best described by a Gauss law is too restrictive and not very accurate (see also Lavallée and Archuleta 2003; and Lavallée and Beltrami, 2004).

The Lévy law (also denoted the stable law, Lévy-stable law or the α-stable law in the literature) is the most general law for which the Central Limit theorem applies —specifically the sum of (independent and identically distributed —iid) Lévy random variables is also distributed according to a Lévy law. The Lévy law is characterized by four parameters α, β, γ and μ. The parameter α, with $0 < \alpha \leq 2$, controls the rate of falloff of the tails of the probability density function. The larger the value of α, the less likely it is to find a random variable far away from the central location. The case $\alpha = 2$ corresponds to the Gaussian distribution; the case $\alpha = 1$ with $\beta = 0$ corresponds to the Cauchy distribution. The parameter β, with $-1 \leq \beta \leq 1$, controls the departure from symmetry of the PDF curve. When $\beta = 0$, the PDF is symmetric and centered about μ. The parameter γ, $\gamma > 0$, is mainly responsible for the PDF width. When $\alpha = 2$, the

parameter γ is related to the variance σ^2 of the Gaussian distribution by $\gamma = \sigma^2/2$. The parameter μ is the location or shift parameter. When $\alpha = 2$, then μ corresponds to the mean value, and when $\alpha = 1$ (with $\beta = 0$) it corresponds to the location parameter of the Cauchy distribution. (See also the Appendix for more details)

The basic difference between a Gaussian distribution and an Lévy distribution can be illustrated by comparing the distribution of heights with the distribution of annual incomes for American adult males (Montroll and Shlesinger, 1983). An average individual who seeks someone twice or three times his height would likely fail. On the other hand, it would not be difficult to find a person with twice or three time one's income. Systems at equilibrium or near the equilibrium are often devoid of large fluctuation —this is the reason why they remain at equilibrium— and can be (although not necessary) described by the Gaussian law. However, non-equilibrium system are characterized by large fluctuations that can be best accounted by a Lévy law. It should not be a surprise that earthquake slip or pre-stress belongs to the latter because the slip is inferred from ground motion recordings following a major earthquake —a truly non-equilibrium phenomenon.

There are two assumptions made in the application of this stochastic model to experimental data. First, we assume that the Lévy PDF are truncated, indicating that random variables are bounded between minimum and maximum values. However, we do assume also that these values are large enough so that the Central Limit theorem still applies (see Paul and Baschnagel, 1999 and references therein for a discussion on the validity of the Central Limit theorem for truncated Lévy random variables; for an interesting discussion of the "unbounded" nature of probability law such as the Lévy law see the Introduction in Nikias and Shao, 1995).

A common feature exhibited by "complex data" in seismology (or related disciplines) is the presence of scaling laws. Accurate computation of such power law and the range of its validity are still open to debate. The second hypothesis adopted in this study, is that the scaling law can only be observed and computed in average. The scaling law doesn't have to be observed locally, that is, at a particular location, over a set of sub-faults or layers of the slip spatial distribution. Local deviations from the scaling law are expected for a finite —or small enough number— of events. Borrowing

from the terminology and conceptualization used in statistical physics, we assumed that the scaling law is "canonical", i.e. that it can be only properly observed and computed when averaged over many events. In a canonical description of the statistical properties of a system, the average energy is conserved, while in a micro-canonical description the energy is exactly preserved everywhere in the system. Note also that this requirement is rather typical for processes described by fBm or similar random processes. The concept of canonical and micro-canonical descriptions have also been discussed in the context of another stochastic model called cascade processes (for instance see Lavallée *et al.*, 1991).

Within these restrictions, the model outlined above can be applied to any data set that is characterized by a spectrum with a power law behavior (for details see Sections III and IV below) such as paleoclimatic (Lavallée and Beltrami, 2004).

III ONE-DIMENSIONAL STOCHASTIC MODEL

III a Formulation of the stochastic model

The stochastic model proposed here consists of a convolution in the Fourier space between the Fourier transform of random variables (white noise) X and some function with a power law dependence $k_x^{-\nu/2}$ where k_x is the horizontal wave number. The scaling exponent ν measures the departure from the non-correlated random variable (white noise when $\nu = 0$). This stochastic process is similar to a fractional Brownian motion that reduces to a random walk in its simplest manifestation —with $\nu = 2$ and X a Gaussian random variable (Peitgen and Saupe, 1988; and Falconer, 1990). In one dimension, the stochastic model Y_x is given by the following relationship:

$$Y_x \propto \sum_{s=2-N/2}^{1+N/2} \left| k_x / 2\pi \right|^{-\nu/2} F_s[X_x] \exp[-2\pi i (x-1)(s-1)/N] , \qquad (1)$$

for a set of random variables X_x distributed over a one–dimensional lattice of length N, where x is the integer spatial variable on the one-dimensional lattice. The discrete variable s is related to k_x by $k_x = 2\pi(s-1)/N$; $F_s[X_x]$ is the discrete Fourier transform of the random variables (for $s \le 0$ in Eq.

(1), the index $s = N + s$ in $F_s[X_x]$). We assume that $k_x^{-\nu/2} F_s[X_x] \to 0$ at $s = 1$. According to this formulation, the power spectrum $P(k_x)$ associated to Y_x will be given by the following relation:

$$P(k_x) = |F_s[Y_x]|^2 \propto k_x^{-\nu} \tag{2}$$

This equation can be used to compute the values of the parameter ν associated to Y_x. Using this scaling exponent the underlying random variables X_x associated to a stochastic model Y_x can be computed by using the following relationship:

$$X_x \propto F_x^{-1}[F_s[Y_x] \times k_x^{\nu/2}], \tag{3}$$

where F_x^{-1} is the Fourier inverse. The one point statistical properties of the stochastic model are completely specified when the probability law and parameters governing X_x are identified. The probability law controls the variability of the stochastic model while ν constraints its long-range correlation.

III b Stochastic modeling of earthquake source models

In this section we discuss the computation of the parameters of the stochastic model for the dip and strike slips for four earthquakes. There are several features that distinguish our computation from the stochastic modeling discussed in Somerville *et al.*, (1999) or Mai and Beroza (2002). First both have interpolated data before performing their statistical analysis. The interpolation creates additional correlations in the data and lead to a spurious estimation of the scaling exponent (for discussion and illustration see Lavallée and Archuleta, 2003). The second difference is a consequence of the interpolation: their analysis is performed in 2D, a luxury that one does not have when sticking to the original slip distribution (except for the Northridge source model that will be considered in the next section). A third difference is that they model the vector sum of the slip amplitude while we consider both the dip and strike slip amplitudes separately. There is no fundamental reason motivating our choice. However, analyses of the dip and strike slip provide more data to analyze and to validate the stochastic model. This procedure allows comparing how the parameters of the stochastic model vary with the direction. A cursory comparison of the dip and

strike slip computed for the Imperial Valley earthquake in Archuleta (1984) shows that the difference between the two can be quite important. (There is almost no spatial variability in the inverted dip slip, with most of the sub-faults having zero dip slip. The absence of many sub-faults with values different from zero in this data set makes it difficult to derive a reliable estimate of the PDF, which is why the dip slip is not considered in our study).

The dip and strike slip spatial distributions of the 1989 Loma Prieta, the 1994 Northridge and 1995 Hyogo-ken Nanbu (Kobe) earthquakes (see Figures 1 to 3), as well as the strike slip of the 1979 Imperial Valley earthquake (Figure 4), have been analyzed according to the following procedure.

The power spectrum $P(k_x)$ is computed for each of the horizontal layers illustrated in Figures 1 to 4. For both, the dip and the strike slip, the mean power spectrum of the horizontal layers has been computed —see Figures 5a and 5b. For each distribution, the spectrum show that there are no dominating wave numbers, which suggest that the data cannot be reduced to—or understood as— a combination of several periodical functions. The curves illustrated in Figures 5a and 5b show that all the wave numbers contribute to the slip variability but also that the weight of the wave numbers approximately follows a trend given by a decaying power law. The values of the scaling exponents ν are reported in Tables 1 and 2 for the dip and the strike slip distributions, respectively**.**

After estimating the parameter ν, each layer of the slip spatial distribution is filtered in the Fourier space in such a way that the resulting field has a mean power spectrum behavior that follows a flat curve (white noise). We assume that the resulting field corresponds to a field of random variables of magnitude X and compute the probability density function (PDF) of X. The (discrete) PDFs are illustrated in Figures 6 to 12 for both, the dip and strike slip distributions of the four earthquakes mentioned above.

The final step consists in determining the probability law that will provide the best fit to the PDFs illustrated in Figures 6 to 12. Three candidates are considered: the Gauss law, the Cauchy law and the more general Lévy law. The method to compute the parameters is discussed in the

Appendix. For each earthquake, the parameters of the best fitting Gaussian, Cauchy and Lévy laws are listed in Tables 1 and 2. The curves of the Gaussian, Cauchy and Lévy laws that best fit the PDF are reported in Figures 6 to 12. For each slip distribution used in this study, the Lévy law provided the best fit to the PDF. For almost all of the available slip distributions, the Cauchy law provides a better fit than the Gauss law except for the dip and strike slip of the Hyogo-ken Nanbu (Kobe) earthquake. In Figures 6 to 12, comparison of the tails of the PDF to the tail of the best fitting Cauchy, Gaussian and Lévy curve confirms that the Lévy law provides a better fit.

In computing the PDF associated with the Imperial Valley slip distribution (see Figure 8), we purposely choose to compute the PDF for an increment in random variable magnitude ΔX (corresponding to the width of the columns in Figure 8) that differs from the one used in Lavallée and Archuleta (2003). The motivation for this choice was to get a rough estimate of the variation in the PDF parameters due to a change in the computed PDF. In Lavallée and Archuleta (2003), ΔX was set to 2.5 but is equal to 3.0 in this paper. In this paper, we assume that the probability density function iss symmetric ($\beta = 0$); so only three parameters were determined. Comparing the values on the four Lévy parameters for both width increments 2.5 and 3.0, we obtained respectively values of 0.92 and 1.14 for α, 0.0 and 0.04 for β, 3.75 and 2.75 for γ, and values of –1.0 and –0.42 for μ. The order of magnitude of each parameter is similar for both computations. These numerical computations give an indication of the accuracy of the parameters values estimated (see also the Appendix for questions related to the accuracy of the estimated parameters).

For the seven samples under study, we found that the power spectrum behavior can be approximated by a power law behavior, although the accuracy of this approximation varies from one sample to another (see the discussion in Figure caption 5). The scaling exponent ν takes values between 0.78 and 1.71. For the three earthquakes for which analysis of slip in both the dip and strike direction were performed, only the Northridge earthquake has a scaling exponent that varies significantly (see Tables 1 and 2) between the two directions. This would suggest a higher correlation in the strike direction.

There are variations in the values of the Lévy parameters computed for the seven samples under study. When comparing the values of the parameters α for the dip and the strike direction of these tree earthquakes, we found no significant difference. The parameter α takes values close to 1, except for Hyogo-ken Nambu earthquake, where the values are around 1.5. This suggests that the frequency of large slip events —asperities or large stress drop— decays at a faster pace for this earthquake when compared to the other three earthquakes. The values taken by the parameter β indicated significant departure from a symmetric PDF for both slip distributions (along dip and along strike) of the Loma Prieta earthquake and the strike slip of the Hyogo-ken Nanbu earthquake. For the Loma Prieta, Hyogo-ken Nanbu and the Northridge earthquakes, the values of the γ parameters associated to the dip slip are systematically larger that the ones computed for the strike slip. For both the dip slip and the strike slip, the values of γ decay from a maximum for the Loma Prieta earthquake, followed by the Hyogo-ken Nanbu and the Northridge earthquake. There is no simple interpretation of the variation in the values of γ when going from one earthquake to another, since one or several parameters such as α, β and ν are varying significantly from one sample to another. (It should be noted that the values estimated for the parameter γ will depend on the definition adopted for the inverse Fourier transform used in Eq. (3), but this definition will not affect the values computed for α and β.) Finally note that for $s = 1$, $k = 0$ in the convolution given by Eq. (3). This implies that the average value of the random variables estimated with Eq. (3) will be zero. This will affect the values taken by the location parameter μ and suggests that not too much importance should be granted to the values taken by μ.

Variation in the model parameters from one earthquake to another may suggest dependence in the fault physical properties. It may also point to some important difference in the process governing the propagation of rupture from one earthquake to another. However, the variation may also reflect, at least partially, the presence of additional noisy effects and other uncertainties in the data. The source models used in this study were computed by using different algorithms. The algorithm itself may be a cause for variations in computing the model parameters —for instance due to the inclusion of interpolation techniques (Liu and Archuleta, 2004) or the directivity effect

(Sekigushi et al. 2002) in the inversion. Further investigations are needed to reach a definitive conclusion. Nevertheless these results also show that the stochastic model described at the beginning of this section, can be used to compute the one-point and two-points statistics of several earthquakes.

IV TWO-DIMENSIONAL STOCHASTIC MODEL

IV a Formulation of the stochastic model

In the previous section, we presented the results of our analysis of the statistical properties of the earthquake source models in term of a one-dimensional stochastic model. The stochastic model is based on the assumption that the horizontal layers are statistically independent one from the other. This assumption is not completely accurate. For instance, computation of the 2D Fourier amplitude of the dip and strike slip of the Northridge earthquake suggests that the 2D Fourier amplitude is function of the wave number amplitude $k = |\mathbf{k}| = \sqrt{k_x^2 + k_y^2}$, with $\mathbf{k}$ the 2D wave number vector; k_x and k_y are horizontal and vertical wave numbers, respectively (see Figure 13). To investigate the dependence on the wave number amplitude, we can make the assumption that the slip distribution is isotropic and that the spectrum is only function of k (see also Mai and Beroza, 2002 for a discussion on this issue). Conversely, this will imply that the correlation function —i.e. two-points statistics— is only function of the distance between the two points and not of the direction. This assumption, as the one discussed in the previous section, can be understood as first order approximations. Both assumptions are probably too simple to take into full account all the complex features included in the source model (see Figure 13). However, there is no theoretical model available for the correlation function of the spatial slip distribution. Furthermore, empirical derivation of a more sophisticated functional behavior for the correlation function —or spectrum— is hardly possible due to the low number of sub-faults computed in source models, The only available alternative to the assumption that the horizontal layers are statistically independent is the assumption that the slip distribution is isotropic. In this section, we derive a stochastic model for the

Northridge slip distribution based on the assumption that the correlation is isotropic. The goal of this exercise is to be able to appreciate the correctness of the description of the slip magnitude —i.e. one-point statistic— in term of a Lévy distribution under these two assumptions. We are also interested in comparing how the parameter values change as a function of the 1D or 2D description.

The one-dimensional stochastic model discussed in Section IV can be easily generalized to a two-dimensional isotropic stochastic model by following the procedure used to generalized one-dimensional fBm to two-dimensional fBm (Peitgen and Saupe, 1988; and Falconer, 1990). In two dimensions, the stochastic model $Y_{x,y}$ is given by the following relationship:

$$Y_{x,y} \propto \sum_{t=2-N/2}^{1+N/2} \sum_{s=2-N/2}^{1+N/2} (k/2\pi)^{-\nu/2} F_{s,t}[X_{x,y}] \exp[2\pi i(x-1)(s-1)/N] \exp[2\pi i(y-1)(t-1)/N], \quad (4)$$

for a set of random variables $X_{x,y}$ distributed over a two–dimensional square lattice of size N, where x and y are the integer spatial variables on the two-dimensional lattice with the distance $r = \sqrt{x^2 + y^2}$. Both sums in equation (4) go from 1 to N; the discrete variables s and t are related to k by $k = 2\pi\sqrt{(s-1)^2 + (t-1)^2}/N$; $F_{s,t}[X_{x,y}]$ is the two-dimensional discrete Fourier transform of the random variables (for $s \le 0$, the index $s = N + s$ and for $t \le 0$, the index $t = N + t$ in $F_{s,t}[X_{x,y}]$). According to this formulation, the power spectrum $P(k)$ associated to $Y_{x,y}$ will be given by the following relation:

$$P(k) = \left|F_{s,t}[Y_{x,y}]\right|^2 \propto k^{-\nu} \quad (5)$$

As for the one-dimensional stochastic model, after computing the scaling exponent ν associated to a stochastic model $Y_{x,y}$, the random variables $X_{x,y}$ can be computed by using the relationship:

$$X_{x,y} \propto F_{x,y}^{-1}[F_{s,t}[Y_{x,y}] \times k^{\nu/2}], \quad (6)$$

where $F_{x,y}^{-1}$ is the two-dimensional Fourier inverse.

IV b Stochastic modeling of the 1995 Northridge slip distribution

Assuming an isotropic distribution of heterogeneities, we computed the two-dimensional spectrum, for the dip —and strike— slip distribution of the Northridge earthquake (Figure 2). The behavior of the spectrum is illustrated in Figures 14a and 14b. The values of the scaling exponents are given in Table 3. These values are lower than those reported in the literature. In Somerville *et al*. (1999), the spectrum decays approximately with a scaling exponent of –4, while Mai and Beroza (2002) reported values closed to –3 in a study including many sources models. In these studies, the spectrum was computed with interpolated slip distribution. The interpolation creates additional correlations in the slip distribution, altering the estimate of the power spectrum and the related scaling exponent (see Lavallée and Archuleta, 2003 for a discussion).

The spatial distribution of the random variable X_r is obtained by filtering in 2D (see Eq. 6) the slip distribution. The (discrete) probability density functions are computed and illustrated in Figures 16 and 17. Finally the parameters of the Gaussian, Cauchy and Lévy laws that best fit the PDF are computed following the procedure described in the Appendix. The values of the parameters are given in Table 3. The discrete PDF as well as the curves of the Gaussian, Cauchy and Lévy laws that best fit the PDF are illustrated in Figures 15 and 16.

As for the one-dimensional modeling of the Northridge earthquake, the Lévy law provides the best fit to the computed PDF. In 1D and 2D, the distribution of the random variables is almost symmetric (β close to 0). However, the parameter α takes larger values when compared to the values obtained for the one-dimensional modeling of the Northridge earthquake. Nevertheless, these values are within the range of values reported for all the earthquakes discussed in the previous section. This implies that the one-dimensional model predicts extreme large events —such as asperities— with a higher frequency than the two-dimensional model. It is difficult to assess the reason why we observe such a difference. This may reflect uncertainty in the estimate of the parameter α for this data set (see also the Appendix on this question). To get a better estimate of this parameter, and also to assess the correction of a 1D or 2D stochastic modeling, additional

investigations are needed. For instance, one could analyze in parallel the statistical properties of the source model and the ground motion (see Lavallée and Archuleta, 2004).

Comparison of the values of the parameters γ and μ obtained from a one-dimensional and two-dimension modeling is not relevant (as described in the previous section). The value taken by the parameter γ depends on the constants used in the definition of Eqs. (1) and (4). These constants are not the same and have a different effect on the estimated γ.

The basic idea behind the filtering is to obtain (idd) random variables (white noise) and compute the probability law associated with them. The random noises, computed through the two filtering processes discussed in this paper, are only approximately independent and identically distributed. Nevertheless, comparison of the values of the parameters of the Cauchy, the Gauss and Lévy laws for the 1D and 2D filtering suggests the range of values that parameters of the Lévy law can take under these two simple hypothesis.

V DISCUSSION: CONSEQUENCES OF THE LÉVY LAW

The formulation of the slip and pre-stress variability in term of the Lévy random variables has several interesting consequences. Random variables governed by a Lévy law are the most general case for which the Central Limit theorem applies. According to this theorem, a combination of (iid) Lévy random variables X_1 and X_2 will result in a random variable X that also belongs to a Lévy law:

$$a_1 X_1 + a_2 X_2 \overset{d}{=} aX + b \tag{7}$$

where a, a_1, and a_2 are real constants, b is a real number and the symbol $\overset{d}{=}$ stands for equal in probability distribution —i.e. the random variables $a_1 X_1 + a_2 X_2$ and $aX + b$ have the same probability distribution or probability density function. This implies that the PDF associated with X will differ from the PDF of X_1 or X_2 by a translation along the horizontal axis and a multiplicative constant (Uchaikin and Zolotarev, 1999). This property was called "self-replication"

in Kagan (1994) since "the sum of random stable [Lévy] variables is itself a stable [Lévy] variable."

For any (discrete) location on the grid, Eq. (3) and Eq. (6) can be reduced to a sum of N (iid) Lévy random variables (weighted by constant). According to the Central Limit theorem, the stochastic model Y_x (1D) or Y_r (2D) will have its amplitude distributed according to a Lévy law. Consequently the slip or pre-stress spatial distribution are also distributed according to a Lévy law, although the parameters of the Lévy law — γ and μ — will be function of the position.

Consider now the operation of local average (also know as coarse graining) —that consists in computing average over a space interval smaller than the total length of the grid. This operation applied to a stochastic model Y_t corresponds to a sum of Lévy random variables (weighted by different constants). According to the Central Limit theorem, the amplitude of the resulting field, at a lower resolution, will be also distributed according to a Lévy law, although again the parameters of the Lévy law — γ and μ — will be function of the resolution. Source models for different earthquakes are often computed at different resolutions. To get all the source models at the same resolution, one can compute local averages over those models with a higher resolution. The statistical properties of the slip transformed under such an operation will not be affected. In other words, a description of the slip statistical properties in terms of the stochastic model discussed above guaranties that such properties are similar within the scales for which the spectrum power law behavior remains valid. Computation of the statistical properties of the slip distribution at different resolutions will become almost intractable if the statistical properties of the slip cannot be approximated by a Lévy law. In this case, the statistical properties and in particular the probability law will depend on the resolution of the slip inversion.

The dependence of the slip distribution statistical properties on the resolution has been ignored most of the time. Neglecting this question has consequences worthy of a discussion. Consider the converse, that the slip or pre-stress spatial variability is distributed according to a non-Lévy law. For instance let us assume that it is a uniform law. This is the hypothesis adopted by several authors to reproduce the pre-stress heterogeneities in modeling of rupture propagation

(Boore and Joyner, 1978; and Oglesby and Day, 2003). Under the Central Limit theorem, a sum of (iid) random variables distributed according to a uniform law converges to a Gauss law. This implies that any transformation of a slip spatially distributed according to a uniform law that involves a sum will lead to a slip that differs significantly, in term of its probability law, from the original slip. Examples of such transformations found in the literature include computing the moving average to smooth the field (Oglesby and Day, 2003) and computing interpolations to get the field at higher resolution (Somerville *et al.*, 1999; and Mai and Beroza, 2002). The introduction of a dependency between the slip resolution and the probability law is an artifact created through the manipulation of the data but there is no reason to believe that the same process happens in nature. A subsidiary question is, assuming that through kinematic inversion of ground motions one computes slip variability distributed according to a uniform law at a certain resolution, what kind of probability law will be found at a higher resolution? What kind of transformation is required to relate the probability laws computed at different resolutions?

In seismology, as in geophysics in general, data are collected or inferred at various resolutions either in time or space. To get a statistical description of the observation where the description is independent of the resolution imposes constraints on the choice of probability laws that can be used for such a purpose. If we don't want to specify different probability laws at different resolutions, the properties of the random variables should remain invariant under mathematical transformations that mimic transformations of data from one resolution to an other. Because of the Central Limit theorem, the Lévy random variables have these properties.

The stochastic model discussed in this paper can also be used to generate synthetic slip spatial distribution. Several algorithms have been developed to generate Lévy random variables (Chambers et al., 1976; Grigoriu, 1995; and Nikias and Shao, 1995). Examples of synthetics fields generated by the stochastic model discussed above and comparisons to real data are discussed in Lavallée and Archuleta (2003). Note also, that since an interpolation in the physical space corresponds to an extrapolation in the Fourier space, the stochastic model can be used to simulate the spatial distribution of slip at sub-resolution not currently available through kinematic inversion.

Accordingly, the stochastic model will allows one to generate many samples of slip spatial distributions. Although the samples are characterized by the same model parameters, every sample will be visually different from the others. This is a consequence of the random nature of the model. We also think that it is due to the intrinsic random nature of the earthquake process that source models computed for the same earthquake can be so different from one to another. (Examples of different source models for the same earthquake can be found at the following address: http://seismo.ethz.ch/staff/martin/research/srcmod/srcmod.html; Mai *et al.*, 2003). For instance, consider the following experience where several dice are thrown but only the sum is recorded. Let us assume that, in addition to the number of die, this is the only information made available to the modelers. Based on mechanical laws of motions, one can generate simulations of the rolling dice. For instance if for a pair of dice the observation is seven, then scenarios of rolling dice that provide final combinations, such as one and six, two and five or three and four, are all legitimate although quite different solutions. A similar interpretation may hold for the radiation field generated by the rupture motions. Namely, several combinations of asperities distributed over the faults, statistically equivalent but physically located at different positions, can generate seismic wave radiation that is similar in term of observations or measurements.

This section will not be complete without discussing the caveats and limitations associated to the assumptions and approximations underlying the results discussed in this paper. Ground motion is usually understood has a convolution of source, path and site effects. The effect on the source inversion of propagation through an uncertain crustal structure is a fundamental but a difficult question still debated. In principle, uncertainties in the slip distribution can be partially quantified by comparing the slip distribution computed in different inversions. However, only a few papers have inverted real data using the same method applied to different velocity models (Ji et al., 2002; Liu and Archuleta, 2004). One can also argue that the quality of the available data is not sufficient, or that the number of events is not large enough to achieve a significant description of the statistical properties of the source model. The discussion given in the Appendix provides answers to these questions. Also, it should be noted that "lack" of quality or resolution has not prevented the utilization of

source model in numerical simulations of rupture propagation under heterogeneous conditions (Beroza and Mikumo, 1996; Olsen *et al*, 1997; Nielsen and Olsen, 1999; Peyrat *et al*., 2001; and Favreau and Archuleta, 2003). We already have mentioned the Fourier analysis of the slip distribution computed by Somerville *et al*., (1999) and Mai and Beroza (2002). Using the same data, in principle it should be possible to compute the parameters of the probability law with the same accuracy as the parameters of the correlation functions or Fourier spectrum.

Furthermore, the results reported in Sections III and IV are in good agreement with some results reported in the literature. For instance, in many studies of spatial variability of sonic log of seismic velocity, the computed power spectra decay with a power law behavior characterized by an exponent taking values between 0.5 and 1.5 (Holliger and Goff, 2003 and references therein). This should be compared with the values given in Tables 1 and 2. In studies of the asperities distribution over the fault, it was observed that such distribution must be described by a power law behavior with an exponent of 1 (Fakao and Furumoto, 1985) or 2 (Gusev 1989). The Lévy distribution function is characterized by a "heavy tail" that follows a power law behavior with exponent α. The values of α given in Tables 1 to 3 are within the previously reported values of 1 and 2. In a subsequent paper, Gusev (1992) speculates on the Lévy law as a potential candidate to describe the asperity distribution.

Also not included in the investigation discussed in this paper is the spatial variation in other source parameters such as rise time and rupture velocity. Nor do we consider the effect of the time evolution of heterogeneity. The study of complexity in geophysics is a very difficult task. As far as we know, there are no guidelines or full-proof recipes that will guarantee success in deciphering complexity into a set of relatively simple models. In devising our strategy to investigate earthquake complexity, we have decided to try to isolate the effect of slip and pre-stress spatial heterogeneity. It is a first step. Spatial and time variability in other parameters as well as potential coupling effects between the parameters can be added in future research projects.

VI CONCLUSION

In this study, we investigated the variability of sources models computed for four earthquakes: the 1979 Imperial Valley, the 1989 Loma Prieta, the 1994 Northridge and 1995 Hyogo-ken Nanbu (Kobe). For the four earthquakes, we showed that the average power-spectra of the raw, i.e., non-interpolated, data follow a power law behavior with scaling exponents with values less than -4 (see Tables 1, 2 and 3). These results suggest that the slip distributions are much less correlated than what is commonly found from interpolated data or by assumption, for which the scaling exponent is approximately –4 for the power spectrum. Equally important is that the PDF for the slip amplitudes are non-Gaussian. Non-Gaussian laws, of the Lévy type, are characterized by long probability tails that allow the presence of "extremes", large values of slip —corresponding to asperities— with a frequency of occurrence much more important than with a Gaussian law. This allows for a higher probability of having large slip amplitudes distributed over the fault surface. For a comparison between synthetic earthquake slips based on random variables distributed according to a Cauchy law and a Gauss law see Figure 4 in Lavallée and Archuleta 2003. (The effects on the rupture propagation can be watched on a movie available at http://www.crustal.ucsb.edu/~ralph/rupture/.) These results suggest that some features of the slip heterogeneity are quite general, perhaps "universal," and thus can be formulated in term of the stochastic model discussed in this paper. Five parameters are needed to completely determine the stochastic model: the four parameters of the Lévy law controlling the frequency of occurrence of the slip amplitude and a scaling exponent to specify the correlation.

For the Northridge earthquake, we considered two different assumptions regarding the properties of the spectrum or correlation function. Although in both cases we observe that the slip spatial variability can be approximated by Lévy random variables, the parameters of the Lévy law depend on the assumption and filtering computed to obtain the white noise. It should be noted however that the variation in values computed for the Lévy index parameter α —the parameter characterizing the fall off of the probability density function for large event— is of the same order

of magnitude as the variation observed in computing this parameter from generated Lévy random variables (see the Appendix).

Another outcome is to confirm the random nature of slip and pre-stress spatial distribution. The randomness of the source has been postulated in several papers, and in a fewer number of papers, stochastic models have been inferred and parameterized through comparison with data. There is a consensus that, as far as earthquakes are concerned, Nature is indeed rolling dice. In this paper we have found that it is the case but with one important qualification: the probability law that governs the dice statistic is a Lévy law.

Acknowledgements: We would like to thank H. Sekiguchi for kindly providing the source model for the 1995 Hyogo-ken Nanbu (Kobe) earthquake and J. Steidl for the source model for the 1989 Loma Prieta earthquake. Computations discussed in this paper were performed using *Mathematica* 4.2 and 5.0 (Wolfram Research, Inc., 1999). This research has been supported by SCEC grant No. 572726 as well as UCSB matching funds for SCEC and KECK grant No. 19990997. This is SCEC Contribution number XXX. This is ICS contribution No. XXX.

REFERENCES

Aki, K. Characterization of barriers of an earthquake fault. *J. Geophys. Res.*, **84**, 6140-6148, 1979.

Andrews, D. J. A stochastic fault model 1. Static case. *J. Geophys. Res.*, **78**, p. 3867-3877, 1980.

Archuleta, R. J. A faulting model for the 1979 Imperial Valley earthquake. *J. Geophys. Res.*, **89**, 4559-4585, 1984.

Beroza, G. C., and T. Mikumo. Short slip duration in dynamic rupture in the presence of heterogeneous fault properties. *J. Geophys. Res.*, **101**, 22,449-22,460, 1996.

Beroza, G. C., and P. Spudich. Linearized inversion for fault rupture behavior: Application to the 1984 Morgan Hill, California, earthquake. *J. Geophys. Res.*, **93**, 6275-6296, 1988.

Boatwright, J. The effect of rupture complexity on estimates of source size. . *J. Geophys. Res.*, **89**, 1132-1146, 1984.

Boore, D. M., and W. J. Joyner. The influence of rupture incoherence on seismic directivity. *Bull. Seismol. Soc. Am.*, **68**, 283-300, 1978.

Bouchon M., M. Campillo., and F. Cotton. Stress field associated with the rupture of the 1992 Landers, California, earthquake and its implications concerning the fault strength at the onset of the earthquake. *J. Geophys. Res.*, **103**, 21,091-21,097, 1998a.

Bouchon M., H. Sekiguchi, K. Irikura, and T. Iwata. Some characteristics of the stress field of the 1995 Hyogo-ken Nanbu (kobe) earthquake. *J. Geophys. Res.*, **103**, 24,271-24,282, 1998b.

Bouchon M. The state of stress on some faults of the San Andreas system as inferred from near-field strong motion data. *J. Geophys. Res.*, **102**, 11,731-11,744, 1997.

Carlson, J. M., and J. S. Langer. Mechanical model of an earthquake fault. *Phys. Rev. A*, **40**, 6470-6484, 1989.

Chambers, J. M., and C. L. Mallows, and B. W. Stuck. A method for simulating stable random variables. *J. Amer. Stat. Assoc.*, **71**, 304-344, 1976.

Das, S., and Aki, K. A numerical study of two-dimensional spontaneous rupture propagation. *Geophys, J. Roy. Astr. Soc.*, **50**, 643-668, 1977.

Day, S. M. Three-dimensional simulation of spontaneous rupture. The effect of non-uniform Prestress. *Bull. Seismol. Soc. Am.*, **72**, 1881-1902, 1982.

Fakao, Y and Furumoto, M. Hierarchy in earthquake size distribution. *Phys. Earth Planet. Inter.*, **37**, 35-48, 1985.

Falconer, K. Fractal Geometry. Jonn Wiley & sons, Chichester. 288pp., 1990.

Favreau, P. and R. J. Archuleta. Direct seismic energy modeling and application to the 1979 Imperial Valley earthquake, Geophys. Res. Lett., 30(5), 1198, doi:10.1029/2002GL015968, 2003.

Feller, W. An introduction to probability theory and its applications. Vol. II, John Wiley, New York. 669 pp., 1971.

Fricsh, U. Turbulence. Cambride University Press. 296pp., 1995.

Gradshteyn, I. S. and I. M. Ryzhik. Table of integrals, Series, and Products. Fifth ed., Academic Press, Inc., Boston.1204pp, 1994.

Grigoriu, M. Applied Non-Gaussian Processes. PTR Prentice Hall, Englewood cliffs, NJ. 442pp., 1995.

Guatteri, M., P. M. Mai, G. C. Beroza, J. Boatwright. Strong ground motion prediction from stochastic-dynamic source models. *Bull. Seismol. Soc. Am.* **93**. 301-313, 2003.

Gusev, A., A. Peak factors of Mexican accelerograms: Evidence of a non-Gaussian amplitude distribution. *J. Geophys. Res.*, **101**, 20,083-20,090, 1996.

Gusev, A. A. On relation between earthquake population and asperity population on the fault. *Tectonophysiscs*, **211**, 85-98, 1992.

Gusev, A. A. Multiasperity model fault model and the nature of short-periods subsources. *Pure Appl. Geophys.*, **136**, 515-527, 1989.

Gutenberg, B. and C. F. Richter. Earthquake magnitude, intensity, and acceleration, *Bull. Seismol. Soc. Am.*, **3**, 163-191, 1942.

Hartzell, S. H., and T. H. Heaton. Rupture history of the 1984 Morgan Hill, California, earthquake from the inversions of strong ground motion records. *Bull. Seismol. Soc. Am.*, **76**, 649-674, 1986.

Herrero, A. and P. Bernard. A kinematic self-similar rupture process for earthquake. *Bull. Seismol. Soc. Am.*, **84**, 1216-1228, 1994.

Hoffman-Jorgensen, J. Stable densities. *Theory of probability and its applications*. **38**, 350-355, 1993.

Holliger, K. and J. A. Goff. A generic model for the 1/f-nature of seismic velocity fluctuations. In Heterogeneity in the Crust and the Upper Mantle, eds. J. A. Goff and K. Holliger, Kluwer Academic, NewYork, 131-154, 2003.

Ji, C., D. J. Wald, and D. V. Helmberger, Source description of the 1999 Hector Mine, California, earthquake, Part II: Complexity of slip history, *Bull. Seism Soc. Am.*, *92*, 1208-1226, 2002.

Kagan, Y. Y. Distribution of incremental static stress caused by earthquakes, *Nonl. Pr. Geophys.*, **1**, 172-181, 1994.

Lavallée, D., and R. J. Archuleta. On the principle of superposition, the Central Limit theorem, and the coupling of random properties in the source and the ground motion. 2004 SCEC Annual Meeting, Proceedings and Abstracts, Vol. XIII, Southern California Eartquake center, USC. 120-121, 2004.

Lavallée, D. and H. Beltrami, 2004. Stochastic modeling of climatic variability in dendrochronology. *Geophys. Res. Lett.*, **31** (15), L15202 doi:10.1029/2004GL020263.

Lavallée, D. and R. J. Archuleta. Stochastic modeling of slip spatial complexities for the 1979 Imperial Valley, California, earthquake. *Geophys. Res. Lett.*, **30** (5), 1245, doi:10.1029/2002GL015839, 2003.

Lavallée, D., D. Schertzer and S. Lovejoy. On the determination of the codimension function. *Scaling, fractals and non-linear variability in geophysics*. Eds. D. Schertzer, S. Lovejoy , Kluwer, Boston,.p. 99-109, 1991.

Liu, P. and R. J. Archuleta. Inversions for kinematic source parameters of the 1994 Northridge earthquake using a three dimensional velocity structure, *Seism. Res. Lett.* **71**, 220, 2000.

Liu, P-C and R. Archuleta. A new nonlinear finite fault inversion with 3D Green's functions: Application to 1989 Loma Prieta, California, earthquake. *J. Geophys. Res.* **109**, B02318, doi:10.1029/2003JB002625, 2004.

Lomnitz-Adler, J. and P. Lemus-Diaz. A stochastic model for fracture growth on a heterogeneous seismic fault. *Geophys. J. Int.*, **99**, 183-194, 1989.

Madariaga, R. and A. Cochard. Seismic source dynamics, heterogeneity and friction. *Ann. Geofis.*, **37**, 1349-1375, 1994.

Mai, P.M., P. Spudich and J. Boatwright: Hypocenter locations in finite-source rupture models, *Seis. Res. Lett*, **74** (2), 208, 2003.

Mai, P. M., and G. C. Beroza. A spatial random-field model to characterize complexity in earthquake slip. *J. Geophys. Res.*, *107* (B11), 2308, doi:10.1029/2001JB000588, 2002.

Marsan, D. The role of small earthquakes in redistributing crustal stress. Submitted to *Geophys. J. Int.*, 2004.

Mikumo, T., K. B. Olsen, E. Fukuyama and Y. Yagi. Stress-breakdown time and slip-weakening distance inferred from slip_velocity functions on earthquake faults. *Bull. Seism. Soc. Am.*, **93**, 264-282, 2003.

Montroll , E. W., and M. F. Shlesinger. On the wedding of certain dynamical processes in disordered complex materials to the theory of stable Lévy distribution functions. Lectures Notes in Math, **1035**, Spinger, New York.,109-137, 1983.

Nielsen, S. B. and K. B. Olsen. Models of the 1994 Nothridge, California, earthquake: dynamical constraints on stress and friction. *Pure appl. Geophys.*, **157**, ,1999.

Nikias, C. L., and M. Shao. Signal Processing with Alpha-Stable Distributions and Applications. Jon Wiley & Sons, New York. 168pp. 1995.

Oglesby, D. D. and S. M. Day. Stochastic fault stress: Implications for fault dynamics and ground motion, *Bull. Seism. Soc. Am.*, **92**, 3006-3021, 2003.

Olsen, K. B., R. Madariaga, and R. J. Archuleta. Three dimensional dynamic simulation of the 1992 Landers earthquake. *Science*, **278**, 834-838. 1997.

Paul, W and J. Baschnagel. Stochastic Processes. Springer, Berlin. 231pp, 1999.

Peitgen, H-O., and D. Saupe. The Science of Fractal Images. Springer-Verlag, New York. 312pp. 1988.

Peyrat, S., K. Olsen, and R. Madariaga. Dynamic modeling of the 1992 Landers earthquake. *J. Geophys. Res.*, **106**, 26,467-236,482, 2001.

Power, W. L., T. E. Tullis, S. R. Brown, G. N. Boitnott, and C. H. Scholz. Roughness of natural fault surfaces, *Geophys. Res. Lett.*, **14**, ,29-32, 1987.

Rice, J. R. Spatio-temporal complexity of slip on a fault. . *J. Geophys. Res.*, **98**, 9885-9907, 1993.

Rivera, L., and H. Kanamori. Spatial heterogeneity of tectonic stress and friction in the crust. *Geophys. Res. Lett.*, **29** (6), 1245, doi:10.1029/2001GL013803, 2002.

Sekiguchi, H., K. Irikura, and T. Iwata, Source inversion for estimating continuous slip distribution on the fault - introduction of Green's functions convolved with a correction function to give moving dislocation effects in subfaults, *Geophys. J. Int.*, **150**, 377-391, 2002.

Sekiguchi, H., K. Irikura, and T. Iwata, Fault geometry in the rupture termination of the 1995 Hyogo-ken Nambu earthquake, *Bull. Seism. Soc. Am.*, **90**, 117-133, 2000.

Somerville, P., K. Irikura, R. Graves, S. Sawata, D. Wald, N. Abrahamson, Y. Iwasaki, T. Kagawa, N. Smith, A. Kowada. Characterizing crustal earthquake slip model for the prediction of strong ground motion. *Seism. Res. Lett.*, **70**, 59-80, 1999.

Steidl J. H., R. J. Archuleta, and S. H. Hartzell. Rupture history of the 1989 Loma Prieta California, earthquake. *Bull. Seism. Soc. Am.*, **81**, 1573-1602, 1991.

Tumarkin, A. G., and R. J. Archuleta. Stochastic ground motion modeling revisited. *Seis. Res. Lett.*, **68**, 312, 1997.

Uchaikin, V. V., and V. M. Zolotarev. Chance and Stability. VSP, Utrecht, The Netherlands. 570pp, 1999.

Von Seggen, D. A random stress model for seismicity statistics and earthquake prediction. *Geophys. Res. Lett.*, **7**, 637-640, 1981.

Wolfram, S. The Mathematica Book. 5th ed., published by Wolfram media. 1464pp, 2003.

Wyss, M. and J. N. Brune, The Alaska earthquake of 28 March 1964; a complex multiple rupture, *Bull. Seism. Soc. Am.*, **57**, 1017-1023, 1967.

Zeng, Y., and C. Chen. Fault rupture process of the September 20, 1999 Chi-Chi, Taiwan earthquake. *Bull. Seismol. Soc. Am.*, **91**, 1088-1099, 2001.

Zhang, W., T. Iwata, K. Irikura, H. Sekiguchi and M. Bouchon. Heterogeneous distribution of the dynami source parameters of the 1999 Chi-Ch-, Taiwan, earthquake. *J. Geophys. Res.*, **108** (B5), 2232, doi:10.1029/2002JB001889, 2003.

Zolatorev, V. M. On representation of densities of stable laws by special functions, *Theory of probability and its applications.* **39**, 354-362, 1995.

FIGURE AND TABLE CAPTIONS

Figure 1: The fault slip of the 1989 Loma Prieta earthquake obtained through the inversion of strong motion velocity time history (Steidl *et al*., 1991). The slip used in our paper corresponds to Model 14 discussed in Steidl *et al*., 1991. The spatial distribution of the slip was calculated at every 2 km along both the down-dip and the strike directions of the fault surface. The spatial variability of the dip slip (a) and the strike slip (b) are illustrated as colored contours on the fault plane.

Figure 2: The computation of the slip spatial distribution of the 1994 Northridge earthquake is based on the inversion of strong ground motion data (Liu and Archuleta, 2000 and 2004). The spatial distribution of the slip was calculated every 1.7 km along the down-dip direction of the fault surface that extends over 24 km, and every 1.76 km along the strike that extends over 20 km. The spatial distributions of the dip slip (a) and strike slip (b) are mapped onto the fault. Contours of the dip and strike slip illustrate the spatial heterogeneity.

Figure 3: Source inversion of the 1995 Hyogo-ken Nanbu (Kobe) earthquake (Sekiguchi *et al*., 2002) based on strong ground records. The inversion discussed in this paper included the directivity effect. The model fault plane is divided in sub-faults located at 2.05 km intervals in both the strike and the dipping directions. The sub-faults are subdivided in five regions denoted A, B, C, D and E. In the current paper, we only consider the regions A to D. The spatial distributions of the dip slip (a) and strike slip (b) are mapped onto the fault.

Figure 4: A faulting model of the 1979 Imperial Valley earthquake was determined by comparing synthetic particle velocity with near-source strong ground motion (Archuleta, 1984). The spatial distribution of the slip was calculated at every 1.0 km along the downdip

direction of the fault surface that extends from the surface to 13 km and at every 2.5 km along the strike that extends over 35 km. Only the strike slip was used in this study.

Figure 5: Complex systems observed in nature are often characterized by scaling law —for instance the Gutenberg-Richter law for earthquake magnitude (Gutenberg and Richter, 1942), roughness of sliding surface (Power *et al*., 1987) and turbulence (Frisch, 1995). In this paper we investigate the scaling properties associated with dip slip (a) and the strike slip (b) reported in Figures 1 to 4. For each earthquake, the mean power spectrum $P(k_x)$ of the horizontal layers has been computed as a function of the wave number k_x. The mean power spectrum $P(k_x)$ and the best straight line that fits the log-log curve are reported for the slip distributions of the Hyogo-ken Nanbu (hollow black triangle △), the Imperial Valley (green cross ×), the Loma Prieta (hollow blue square □) and the Northridge (hollow red diamond ◊) earthquakes. These results suggest that the scaling behavior is observed for scale length that ranges from 2 to 64 km. The values of the scaling exponents are reported in Tables 1 and 2. The quality of the fitted curves illustrated in (a), as estimated by the values of the linear correlation coefficient (in absolute values), goes from average (0.84 for Loma Prieta) to good (0.94 for Hyogo-ken Nanbu and Northridge). In (b), it goes from poor (0.63 for Imperial Valley), to average (0.85 for Loma Prieta) to good (0.94 for Northridge and 0.96 for Hyogo-ken Nanbu). Fluctuations around the power law behavior can be attributed to a slow convergence to the theoretical curve. The presence of noise (not taken into account by the stochastic model) as well as uncertainties in computing the slip spatial distribution or in recording the ground motions also impinge on the computation of the power spectrum and can be responsible for the departure observed in the plots.

Figure 6: (a) The (discrete) probability density function PDF (red and blue dots and bars) associated to the filtered dip slip X of the Hyogo-ken Nanbu (Kobe) earthquake is compared to the curves of the three probability laws that best fit the PDF: the Cauchy law

(black curve), the Gaussian law (dashed curve) and the Lévy law (green curve). The left side of the PDF ($X < 0$) is colored in red while the right ($X > 0$) side is in blue. The magnitude of the random variables is given by X. The width of the bar corresponding to the increment used to estimate the PDF is 3.5. (b) The left tails of the same curves are illustrated on a log-log plot. (c) The right tails of the curves in (a) are illustrated on a log-log plot. Lévy and Cauchy probability density function are characterized by tails that decay according to a power law. Such behavior is best illustrated on a log-log plot. The misfit of the Gaussian probability density function is more obvious in these plots —see Figures (b) and (c). In particular, note that according to the Gauss law, the large events —last points on the right hand side of the graphics— have almost a zero probability of being observed. The parameters of the Gauss, Cauchy and Lévy laws are reported in Table 1.

Figure 7: Same as Figure 6 but for the random variables associated to the strike slip of the Hyogo-ken Nanbu (Kobe) earthquake. The width of the bar corresponding to the increment used to estimate the PDF is 4. For this case, the shape of the PDF illustrated in (a) is asymmetric with respect to its maximum and best fitted by an asymmetric Lévy law with parameter $\beta \neq 0$ (see also the Appendix). The probability density functions associated with Cauchy and Gauss laws are both characterized by curves symmetric with respect to its maximum. For this reason, the curves of the Cauchy and Gauss laws "overshoot" the extreme events of the computed PDF left tail illustrated in (b). However in (c), we observe that the Gauss law fails to fit the large events. The parameters of the Gauss, Cauchy and Lévy laws are reported in Table 2.

Figure 8: Same as Figure 6 but for the random variables associated with the strike slip of the Imperial Valley earthquake. The width of the bar corresponding to the increment used to estimate the PDF is 3. The remarks discussed in the Figure caption 6 also apply for this

case (see also Lavallée and Archuleta, 2003) The parameters of the Gauss, Cauchy and Lévy laws are reported in Table 2.

Figure 9: Same as Figure 6 but for the random variables associated with the dip slip of the Loma Prieta earthquake. The width of the bar corresponding to the increment used to estimate the PDF is equaled to 10. The remarks discussed in the Figure caption 7 for an asymmetric PDF also apply for this case except that here in the Gauss law is actually providing a good fit to the PDF left tail (b) but completely missed the PDF right tail (c). The parameters of the Gauss, Cauchy and Lévy laws are reported in Table 1.

Figure 10: Same as Figure 6 but for the random variables associated with the strike slip of the Loma Prieta earthquake. The width of the bar corresponding to the increment used to estimate the PDF is 10. The remarks discussed in the Figure caption 9 for an asymmetric PDF also apply for this case. The parameters of the Gauss, Cauchy and Lévy laws are reported in Table 2.

Figure 11: Same as Figure 6 but for the random variables associated with the dip slip of the Northridge earthquake. The width of the bar corresponding to the increment used to estimate the PDF is 7. The remarks discussed in the Figure caption 6 also apply for this case. The parameters of the Gauss, Cauchy and Lévy laws are reported in Table 1.

Figure 12: Same as Figure 6 but for the random variables associated with the strike slip of the Northridge earthquake. The width of the bar corresponding to the increment used to estimate the PDF is 4. The remarks discussed in the Figure caption 6 also apply for this case. The curve associated to the Lévy law underestimate the maximum of the PDF but provides a better fit to the other PDF values. The parameters of the Gauss, Cauchy and Lévy laws are reported in Table 2.

Figure 13: Contour plot of the complex behavior of the Fourier amplitude of the dip (a) and strike (b) slip in the wave number space. The Fourier amplitude is function of the horizontal and vertical wave numbers, respectively k_x and k_y. The large and low values of the Fourier amplitude are in red and blue, respectively. However in (b), contour lines are distributed almost horizontally in a region close to $k_y = 0$, indicating higher correlation along this direction. This suggests that the approximation of the strike slip in term of a one-dimensional stochastic model is more appropriate in this case (see Section III).

Figure 14: The 2D power spectrum $P(k)$ has been computed assuming that the dip and strike slip spatial distributions are isotropic. The square of the Fourier amplitude has been estimated. The results were integrated over a (approximated) circle of radius k with $k = \sqrt{k_x^2 + k_y^2}$. The 2D power spectrum $P(k)$ and the best straight line that fits the log-log curve are reported for the dip slip distributions (hollow black triangle $\triangle$), and the strike slip distribution (hollow blue square $\square$). These results suggest that the scaling behavior is observed for a scale length ranging from 4 to 20 km. The values of the scaling exponents are reported in Table 3. The linear correlation coefficient (in absolute values) takes a value of 0.71 for the dip slip and 0.9 for the strike slip.

Figure 15: Same as Figure 6 but for the random variables associated with the 2D filtering of the dip slip of the Northridge earthquake. The width of the bar corresponding to the increment used to estimate the PDF is 8. The remarks discussed in the Figure caption 6 also apply for this case. The parameters of the Gauss, Cauchy and Lévy laws are reported in Table 3.

Figure 16: Same as Figure 6 but for the random variables associated with the 2D filtering of the dip slip of the Northridge earthquake. The width of the bar corresponding to the increment used to estimate the PDF is 8. The remarks given in the Figure caption 6 also apply for right tail of the curves in (c). There are not enough points to appreciate the fit of for the left tail of the curves in (b). The parameters of the Gauss, Cauchy and Lévy laws are reported in Table 3.

Figure A1: Curves of the Lévy probability density function $p(z;\alpha,\beta,\gamma,\mu)$ for several values of the parameter α: (a) the overall probability density function and (b) the tails of the probability density function. The parameter α is called the Lévy exponent, the characteristic or stable exponent. It controls the rate of fall off of the probability density function as illustrated in (b). Note that by keeping the values of other parameters fixed, the probability to observe random variables with large values increases as α decreases.

Figure A2: Curves of the Lévy probability density function $p(z;\alpha,\beta,\gamma,\mu)$ for several values of the parameter β. The parameter β is called the symmetric or the skewness parameter. It controls departure from symmetry given by $\beta = 0$. Note that for $\beta > 0$, large positive random variables are more likely to be generated. The converse is true for $\beta < 0$ since $p(z;\alpha,\beta,\gamma,\mu) = p(-z;\alpha,-\beta,\gamma,\mu)$.

Figure A3: Curves of the Lévy probability density function $p(z;\alpha,\beta,\gamma,\mu)$ for several values of the parameter γ. The parameter γ is called the scale parameter or dispersion. It controls the width of the probability density function.

Figure A4: Curves of the Lévy probability density function $p(z;\alpha,\beta,\gamma,\mu)$ for several values of the parameter μ. The parameter μ, with $-\infty < \mu < \infty$ is called the location parameter. It shifts the curve to the left or the right.

TABLES

Table 1: Parameters of the stochastic model for the dip slip of three earthquakes. The parameter ν is the scaling exponent of the power spectrum (Figure 3). The parameters of the Gauss, Cauchy and Lévy laws that best fit the PDF(X) in Figures 6, 9 and 11 are given.

	Scaling Exponent	Gauss law		Cauchy law		Lévy law			
	ν	μ	σ	γ	μ	α	β	γ	μ
1989 Loma Prieta	0.94	-8.5	22.	16.4	-10.2	1.31	0.84	34.5	14.3
1994 Northridge	1.18	-1.52	13.9	9.7	-1.13	1.34	-0.05	21.3	-2.2
1995 Hyogo-ken Nanbu	1.47	0.63	9.91	7.3	1.2	1.50	-0.2	18.2	0.2

Table 2: Parameters of the stochastic model for the strike slip of the four earthquakes. The parameter ν is the scaling exponent of the power spectrum (Figure 3). The parameters of the Gauss, Cauchy and Lévy laws that best fit the PDF(X) in Figures 7, 8, 10 and 12 are given.

	Scaling Exponent	Gauss law		Cauchy law		Lévy law			
	ν	μ	σ	γ	μ	α	β	γ	μ
1979 Imperial Valley	0.78	-0.73	4.55	3.3	-0.47	1.14	-0.04	3.75	-1.0
1989 Loma Prieta	1.07	-5.5	19.	13.5.	-8.3	1.07	0.6	15.2	63.7
1994 Northridge	1.71	-0.1	6.3	4.29	-0.56	1.17	0.07	6.41	1.1
1995 Hyogo-ken Nanbu	1.48	-2.2	6.4	4.8	-2.6	1.56	0.85	9.8	0.05

Table 3: Parameters of the 2D stochastic model for the dip and strike slip of the Northridge earthquake. The parameter ν is the scaling exponent of the power spectrum (Figure 14). The parameters of the Gauss, Cauchy and Lévy laws that best fit the PDF(X) in Figures 15 and 16 are given.

	Scaling Exponent	Gauss law		Cauchy law		Lévy law			
	ν	μ	σ	γ	μ	α	β	γ	μ
1994 Northridge dip slip	0.74	-3.8	13.1	10.1	-3.32	1.51	0.2	28.3	-0.9
1994 Northridge strike slip	1.05	1.4	8.	6.1	1.1	1.50	0.2	13.8	2.1

Table A1: Summary of the values obtained for the parameters of the Cauchy, Gauss and Lévy law. The last column reports the values computed for the objective functions given in Eq. (A6). Note that, although we report the values for Eq. (A6) in the sixth line, the parameters reported in these lines where computed by optimizing Eq. (A7). The second line includes the values of the Gauss parameters used to generate the random variables with an algorithm provided with *Mathematica*.

Fitted functions	α	β	γ	μ	Minimum of the objective function in Eq. (A6)
Original values	2	—	2	0.	Does not apply
$p(x;2,\beta,\gamma,\mu)$ (Gauss)	—	—	2.1	0.07	0.154
$p(x;1,0,\gamma,\mu)$ (Cauchy)	—	—	1.51	-0.06	0.338
$\varphi_A(k;\alpha,\gamma)$	2	—	2.09	—	Does not apply
$\varphi(k;\alpha,\beta,\gamma,\mu)$	1.99	1.0	2.08	0.05	0.155
$p(x;\alpha,\beta,\gamma,\mu)$	1.91	0.45	1.99	0.06	0.148

Table A2: Same as Table A1. The second line includes the values of the Cauchy parameters used to generate the random variables with an algorithm provided with *Mathematica*.

Fitted functions	α	β	γ	μ	Minimum of the objective function Eq. (A6)
Original values	1	—	1	0	Does not apply
$p(x;2,\beta,\gamma,\mu)$ (Gauss)	—	—	0.84	0.02	0.379
$p(x;1,0,\gamma,\mu)$ (Cauchy)	—	—	0.97	-0.07	0.226
$\varphi_A(k;\alpha,\gamma)$	1.16	—	0.89	—	Does not apply
$\varphi(k;\alpha,\beta,\gamma,\mu)$	1.15	0.26	0.88	0.93	0.216
$p(x;\alpha,\beta,\gamma,\mu)$	1.04	0.04	0.95	0.45	0.184

Table A3: Same as Table A1. The second line includes the values of the Lévy parameters used to generate the random variables with an algorithm discussed in Chambers *et al*. (1976).

Fitted functions	α	β	γ	μ	Minimum of the objective function Eq. (A6)
Original values	1.5	1	1	0	Does not apply
$p(x;2,\beta,\gamma,\mu)$ (Gauss)	—	—	1.95	-1.17	0.281
$p(x;1,0,\gamma,\mu)$ (Cauchy)	—	—	1.56	-1.32	0.35
$\varphi_A(k;\alpha,\gamma)$	1.59	—	1.51	—	Does not apply
$\varphi(k;\alpha,\beta,\gamma,\mu)$	1.59	1.	1.56	-0.31	0.222
$p(x;\alpha,\beta,\gamma,\mu)$	1.47	1.	1.60	0.22	0.204

Table A4: Same as Table A1. The second line includes the values of the Lévy parameters used to generate the random variables with an algorithm discussed in Nikias and Shao (1995).

Fitted functions	α	β	γ	μ	Minimum of the objective function Eq. (A6)
Original values	1.5	1	1	0	Does not apply
$p(x;2,\beta,\gamma,\mu)$ (Gauss)	—	—	0.7	-0.73	0.384
$p(x;1,0,\gamma,\mu)$ (Cauchy)	—	—	0.88	-0.87	0.375
$\varphi_A(k;\alpha,\gamma)$	1.25	—	0.73	—	Does not apply
$\varphi(k;\alpha,\beta,\gamma,\mu)$	1.26	0.92	0.74	0.81	0.222
$p(x;\alpha,\beta,\gamma,\mu)$	1.25	0.67	0.74	0.45	0.19

Table A5: Same as Table A4.

Fitted functions	α	β	γ	μ	Minimum of the objective function Eq. (A6)
Original values	1.25	0	1	0	Does not apply
$p(x;2,\beta,\gamma,\mu)$ (Gauss)	—	—	1.18	-0.17	0.274
$p(x;1,0,\gamma,\mu)$ (Cauchy)	—	—	1.14	-0.18	0.262
$\varphi_A(k;\alpha,\gamma)$	1.45	—	1.18	—	Does not apply
$\varphi(k;\alpha,\beta,\gamma,\mu)$	1.46	0.47	1.18	0.4	0.191
$p(x;\alpha,\beta,\gamma,\mu)$	1.53	0.4	1.29	0.35	0.168

Table A6: Same as Table A4.

Fitted functions	α	β	γ	μ	Minimum of the objective function Eq. (A6)
Original values	0.8	0	1	0	Does not apply
$p(x;2,\beta,\gamma,\mu)$ (Gauss)	—	—	0.94	-0.13	0.597
$p(x;1,0,\gamma,\mu)$ (Cauchy)	—	—	0.96	-0.13	0.303
$\varphi_A(k;\alpha,\gamma)$	0.84	—	0.99	—	Does not apply
$\varphi(k;\alpha,\beta,\gamma,\mu)$	0.85	-0.14	1.0	0.48	0.301
$p(x;\alpha,\beta,\gamma,\mu)$	0.87	-0.13	0.96	0.38	0.263

Table A7: Same as Table A4.

Fitted functions	α	β	γ	μ	Minimum of the objective function Eq. (A6)
Original values	1.72	0.5	1	0	Does not apply
$p(x;2,\beta,\gamma,\mu)$ (Gauss)	—	—	1.2	-0.19	0.242
$p(x;1,0,\gamma,\mu)$ (Cauchy)	—	—	1.18	-0.36	0.413
$\varphi_A(k;\alpha,\gamma)$	1.65	—	1.1	—	Does not apply
$\varphi(k;\alpha,\beta,\gamma,\mu)$	1.68	1.0	1.1	0.3	0.181
$p(x;\alpha,\beta,\gamma,\mu)$	1.62	0.93	1.16	0.4	0.172

Table A8: Same as Table A1 but for the random variables associated to the dip slip of the Northridge earthquake.

Fitted functions	α	β	γ	μ	Minimum of the objective function Eq. (A6)
$p(x;2,\beta,\gamma,\mu)$ (Gauss)	—	—	96.45	--1.53	0.0321
$p(x;1,0,\gamma,\mu)$ (Cauchy)	—	—	9.69	-1.13	0.0229
$\varphi_A(k;\alpha,\gamma)$	1.34	—	21.12	—	Does not apply
$\varphi(k;\alpha,\beta,\gamma,\mu)$	1.31	-0.1	19.33	-3.57	0.0227
$p(x;\alpha,\beta,\gamma,\mu)$	1.34	-0.05	21.28	-2.16	0.0223

FIGURES

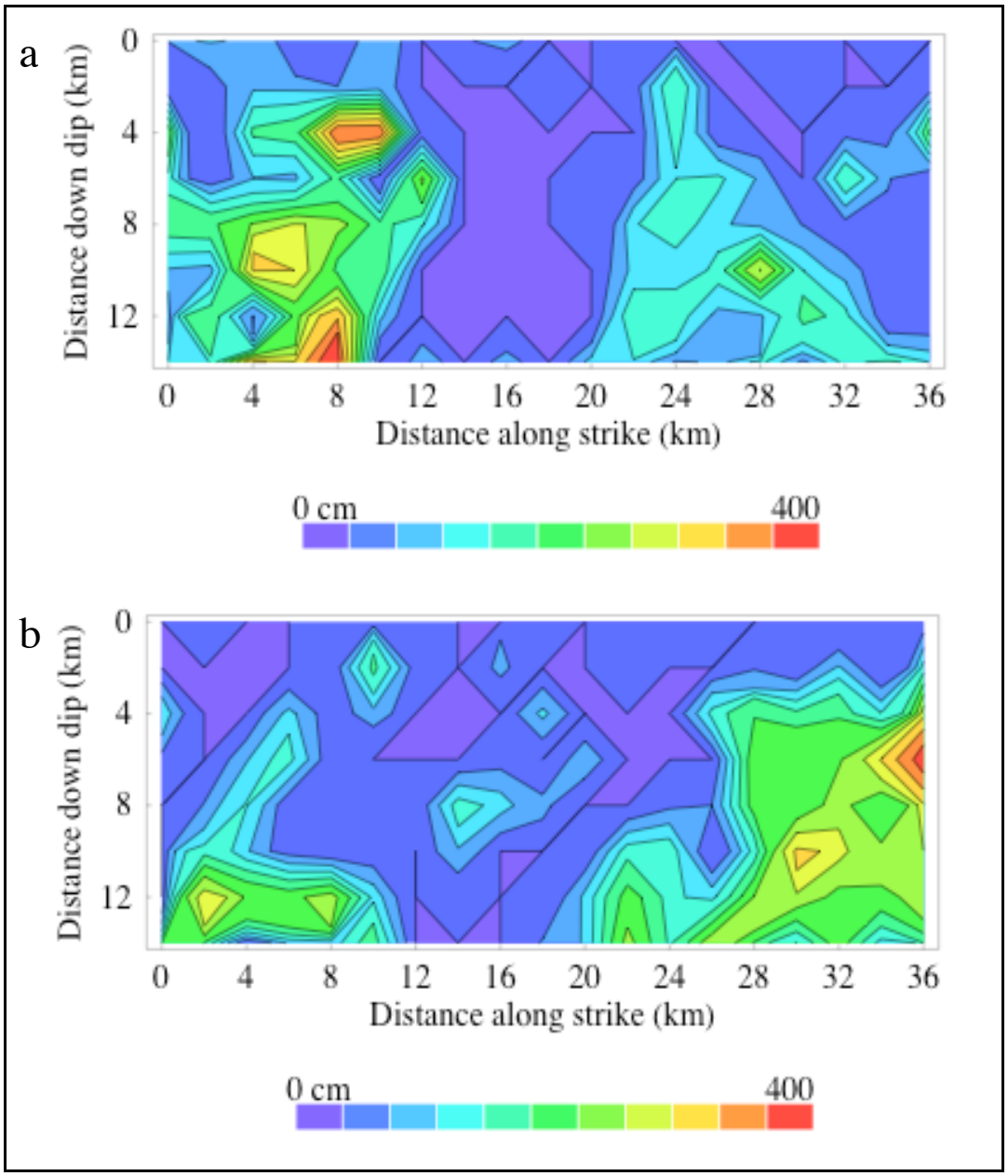

Figure 1:

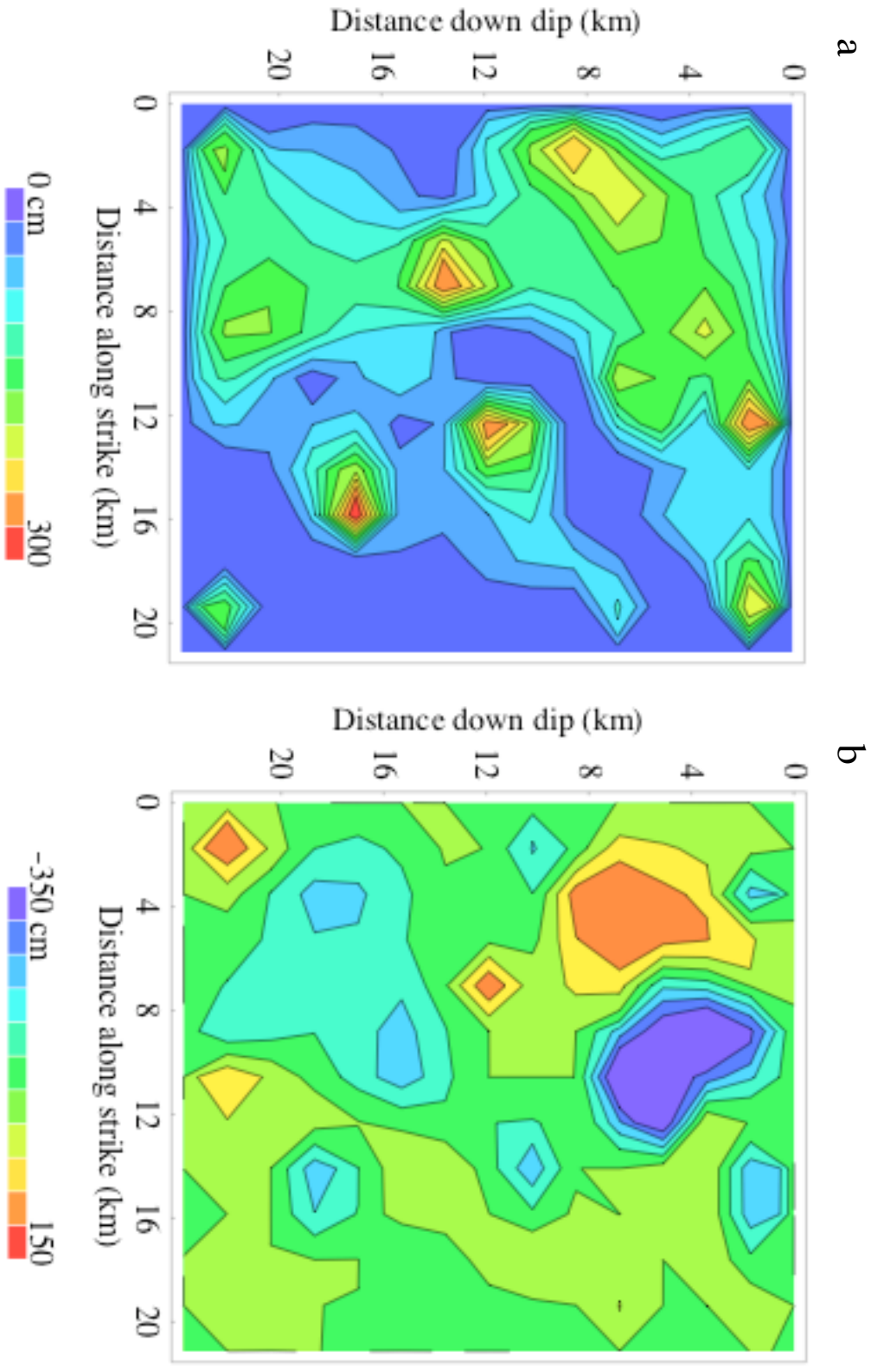
a
Distance down dip (km)
0
4
8
12
16
20
Distance along strike (km)
0
4
8
12
16
20
0 cm
300
b
Distance down dip (km)
0
4
8
12
16
20
Distance along strike (km)
0
4
8
12
16
20
−350 cm
150

Figure 2

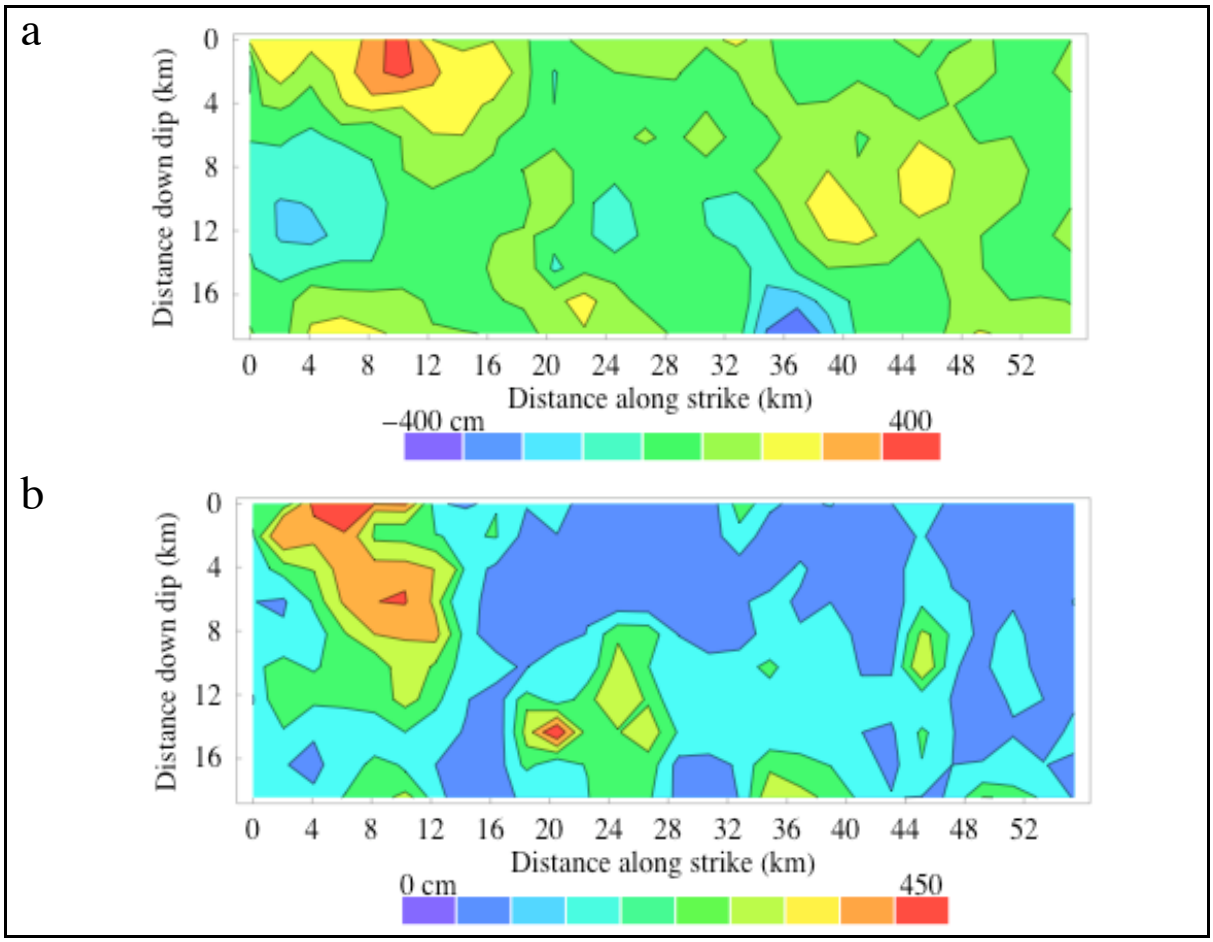

Figure 3:

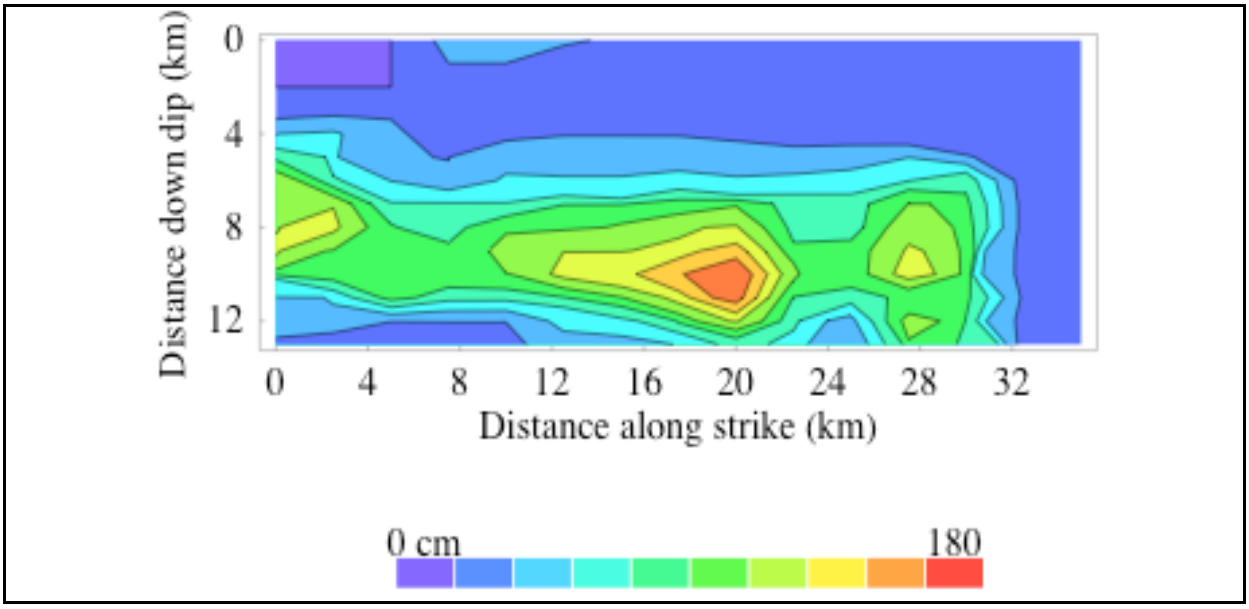

Figure 4:

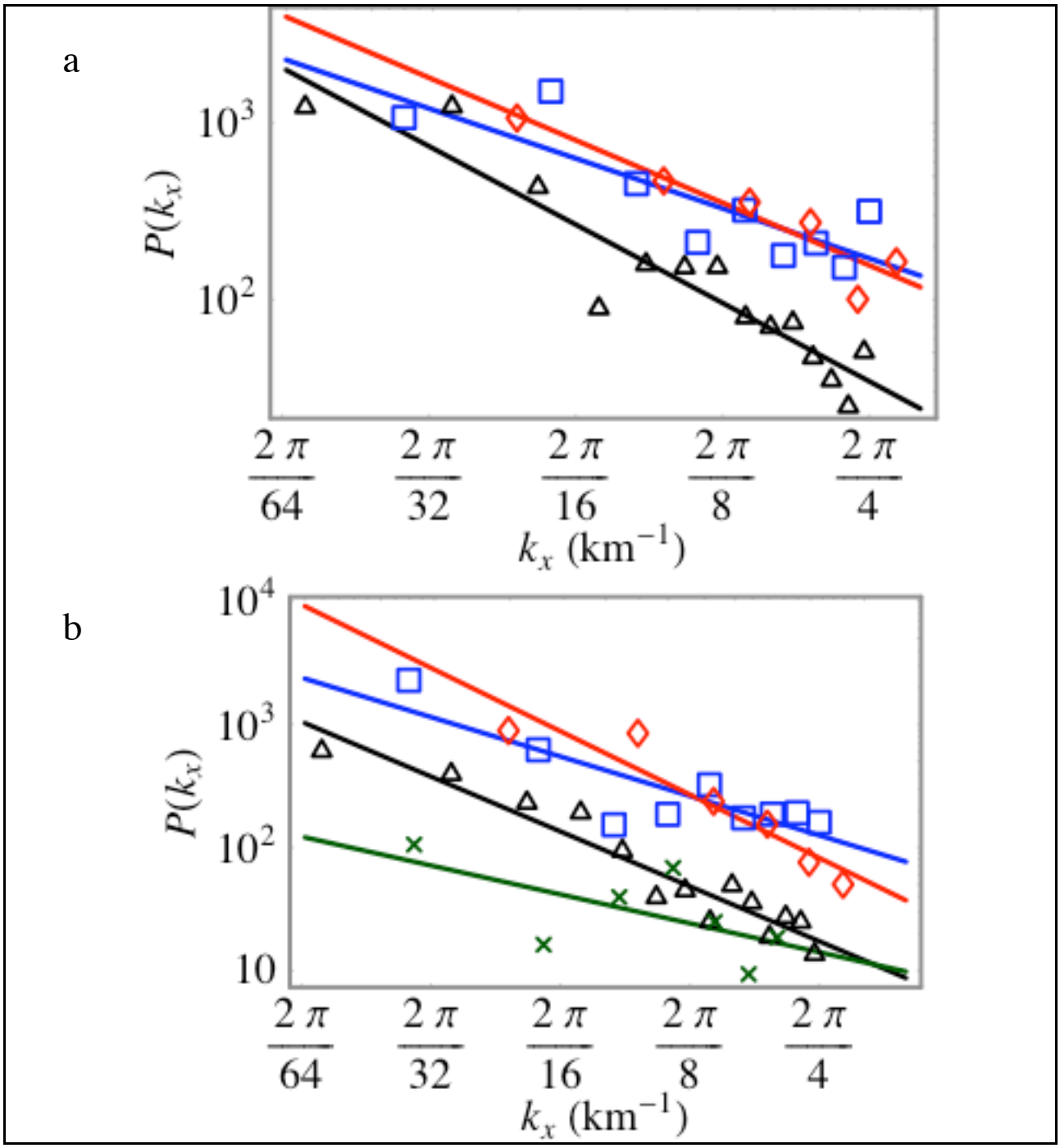
a
10^3
10^2
$P(k_x)$
$\frac{2\pi}{64}$ $\frac{2\pi}{32}$ $\frac{2\pi}{16}$ $\frac{2\pi}{8}$ $\frac{2\pi}{4}$
k_x (km^{-1})
b
10^4
10^3
10^2
10
$P(k_x)$
$\frac{2\pi}{64}$ $\frac{2\pi}{32}$ $\frac{2\pi}{16}$ $\frac{2\pi}{8}$ $\frac{2\pi}{4}$
k_x (km^{-1})

Figure 5:

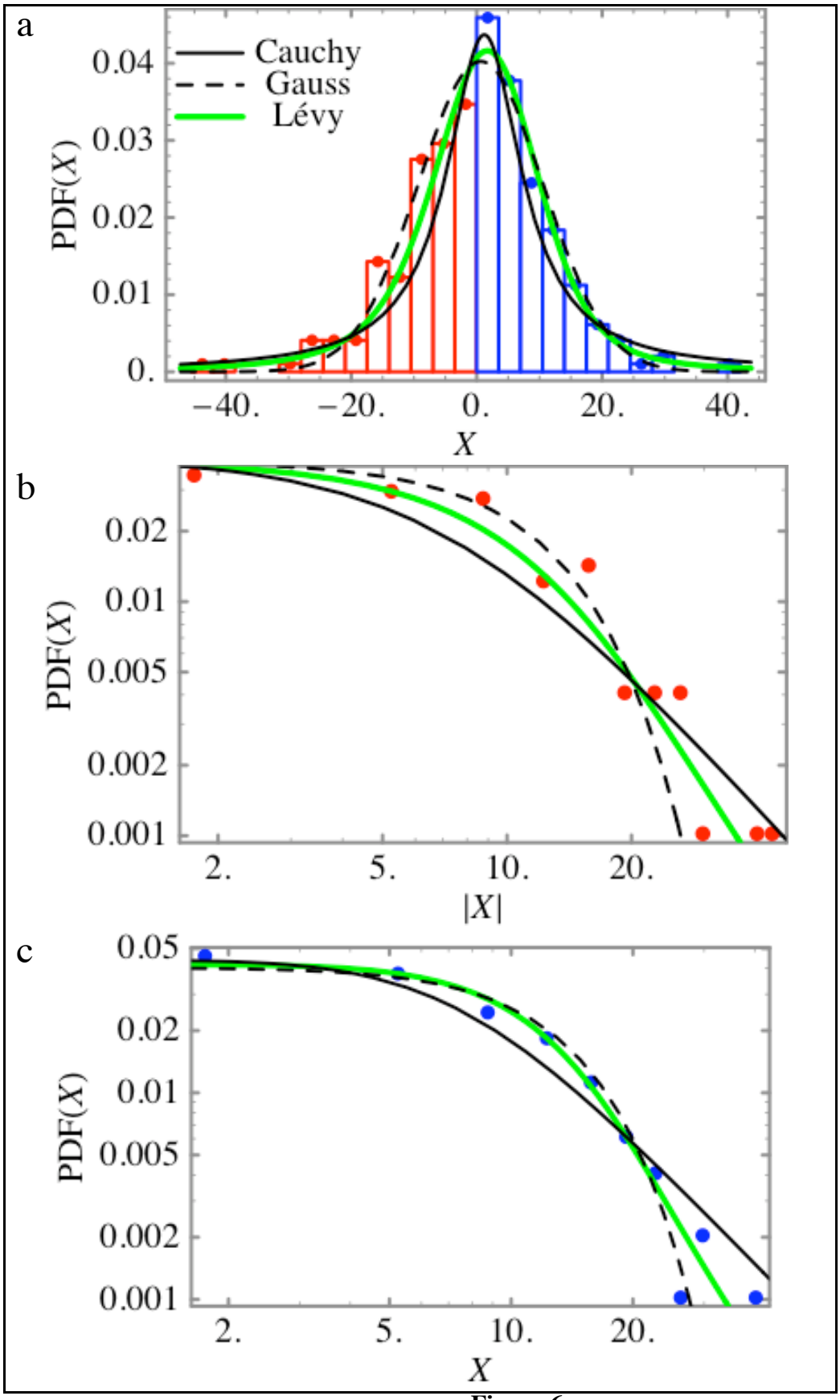
a
Cauchy
Gauss
Lévy
0.04
0.03
0.02
0.01
0.
PDF(X)
−40.
−20.
0.
20.
40.
X
b
0.02
0.01
0.005
0.002
0.001
PDF(X)
2.
5.
10.
20.
|X|
c
0.05
0.02
0.01
0.005
0.002
0.001
PDF(X)
2.
5.
10.
20.
X

Figure 6:

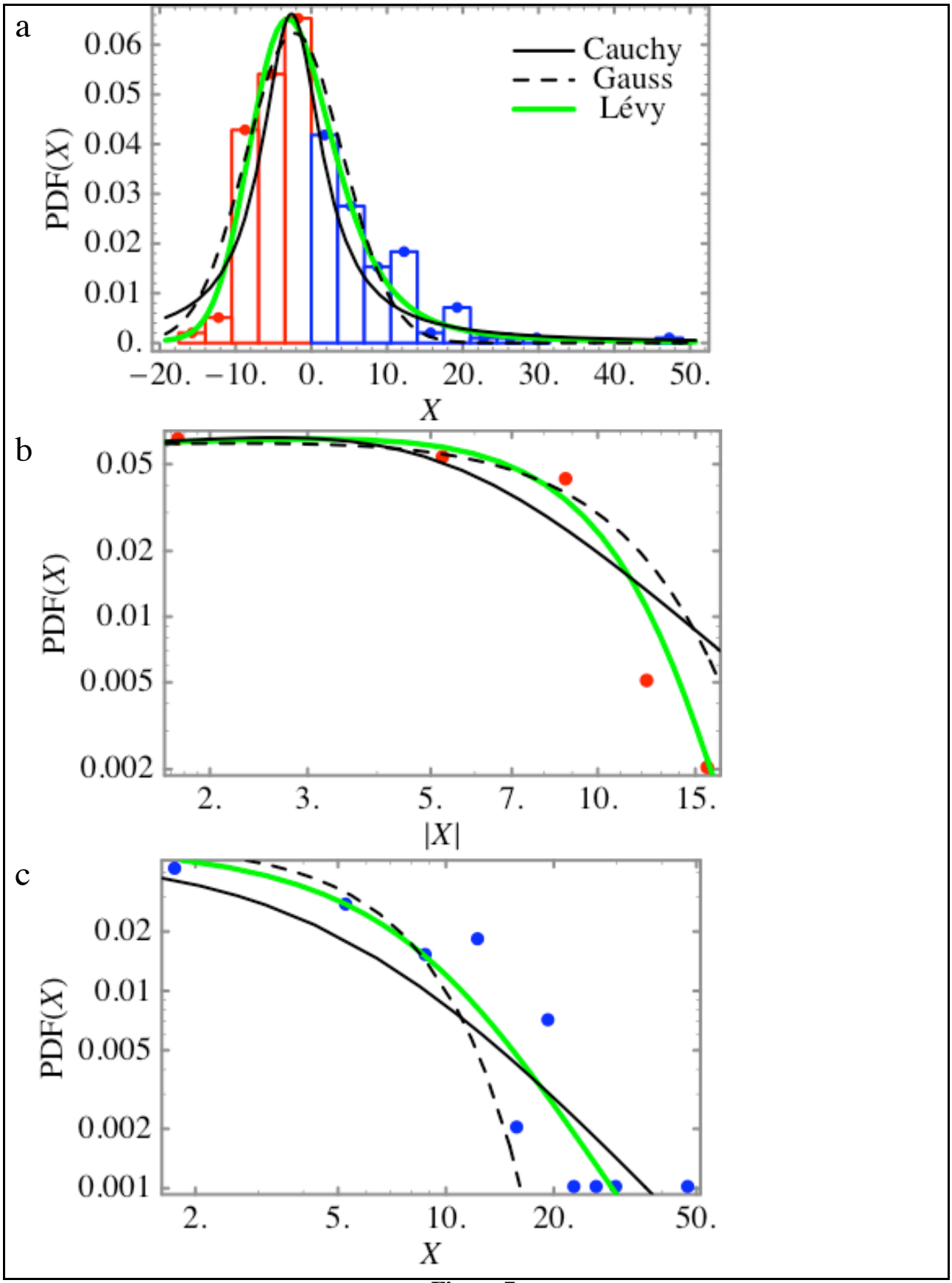
a
0.06
0.05
0.04
0.03
0.02
0.01
0.
PDF(X)
Cauchy
Gauss
Lévy
−20. −10. 0. 10. 20. 30. 40. 50.
X
b
0.05
0.02
0.01
0.005
0.002
PDF(X)
2. 3. 5. 7. 10. 15.
|X|
c
0.02
0.01
0.005
0.002
0.001
PDF(X)
2. 5. 10. 20. 50.
X

Figure 7:

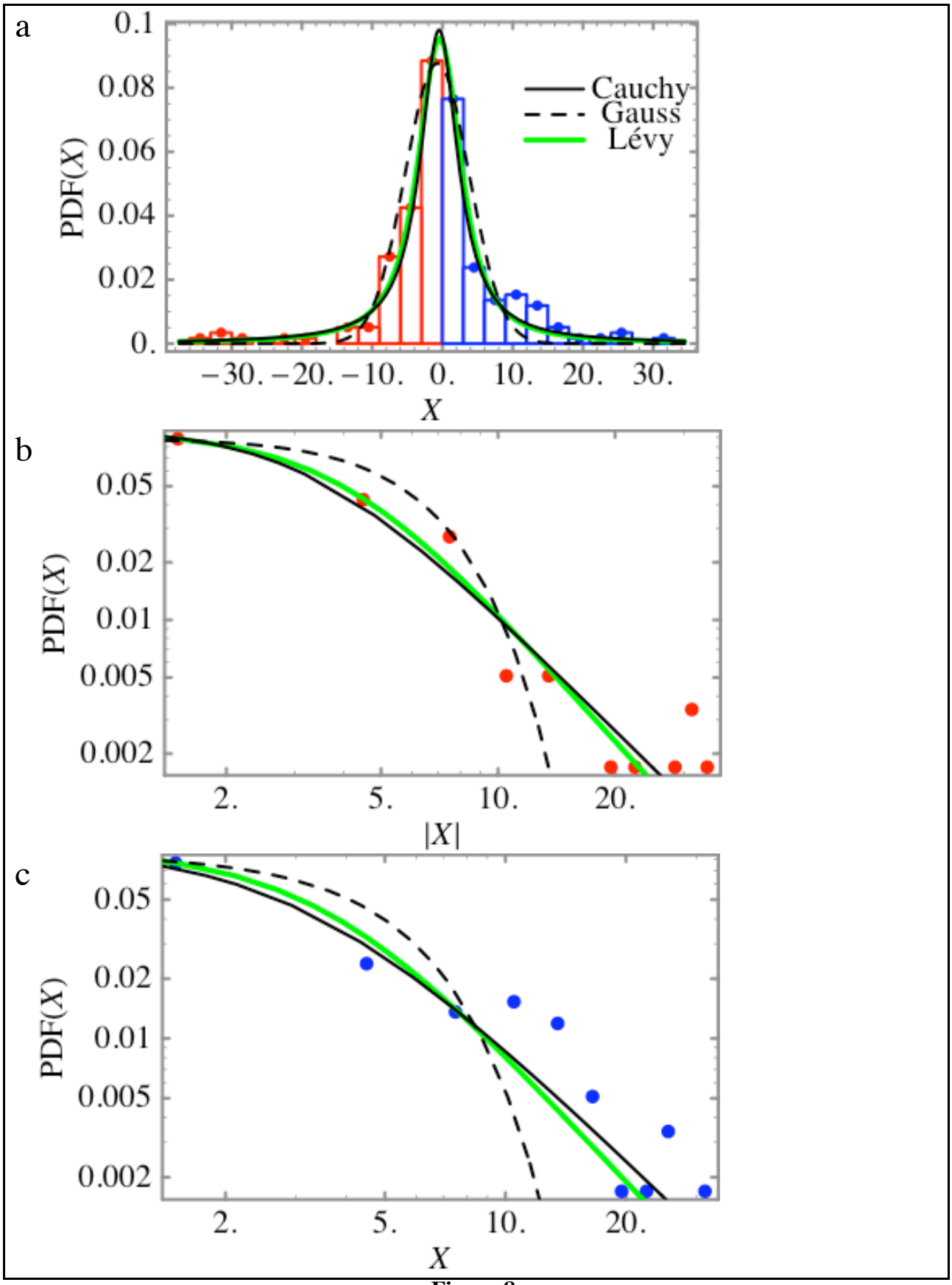
a
0.1
0.08
0.06
0.04
0.02
0.
PDF(X)
Cauchy
Gauss
Lévy
−30.
−20.
−10.
0.
10.
20.
30.
X
b
0.05
0.02
0.01
0.005
0.002
PDF(X)
2.
5.
10.
20.
|X|
c
0.05
0.02
0.01
0.005
0.002
PDF(X)
2.
5.
10.
20.
X

Figure 8:

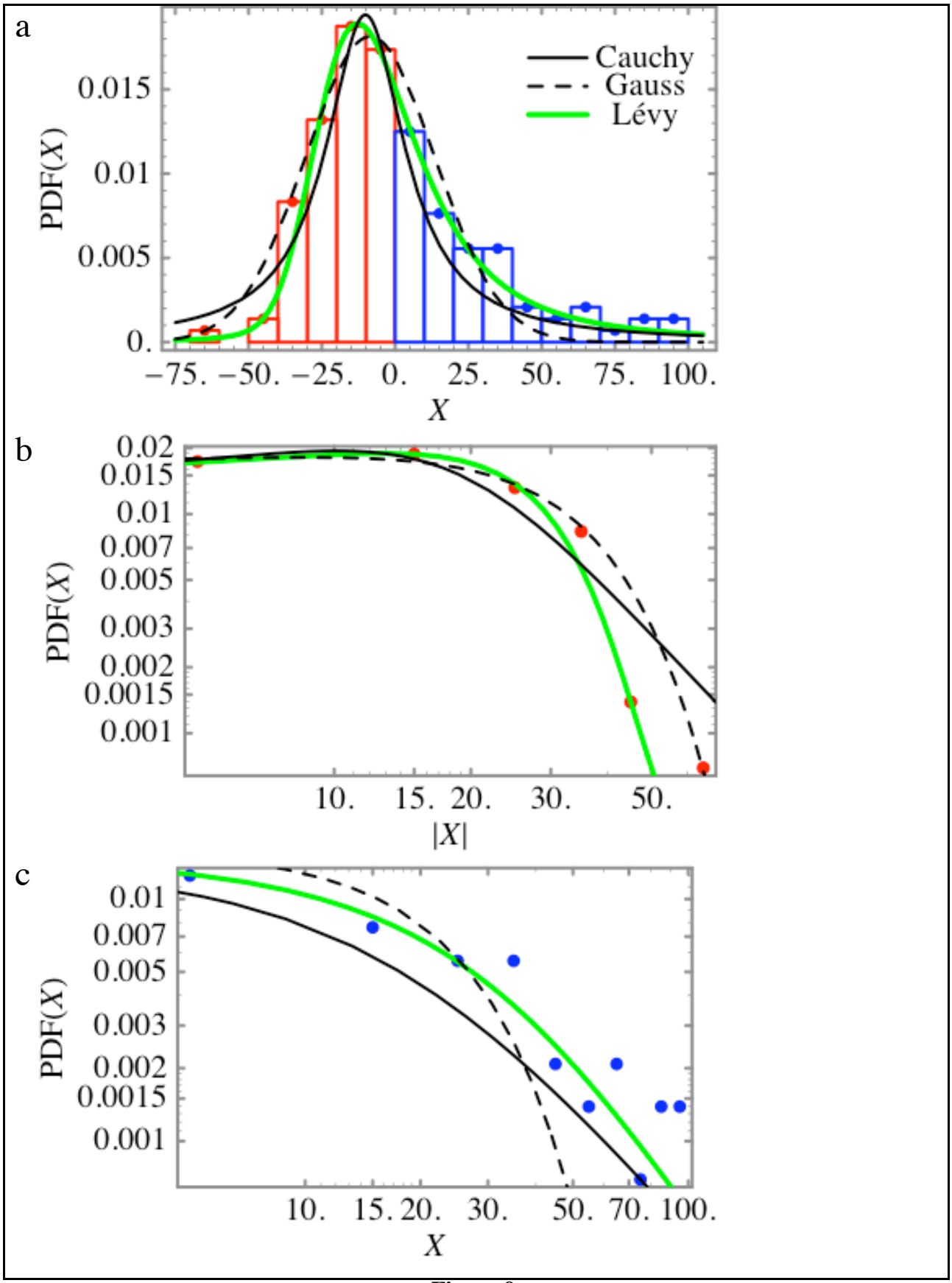
a
Cauchy
Gauss
Lévy
PDF(X)
0.015
0.01
0.005
0.
−75. −50. −25. 0. 25. 50. 75. 100.
X
b
PDF(X)
0.02
0.015
0.01
0.007
0.005
0.003
0.002
0.0015
0.001
10. 15. 20. 30. 50.
|X|
c
PDF(X)
0.01
0.007
0.005
0.003
0.002
0.0015
0.001
10. 15. 20. 30. 50. 70. 100.
X

Figure 9:

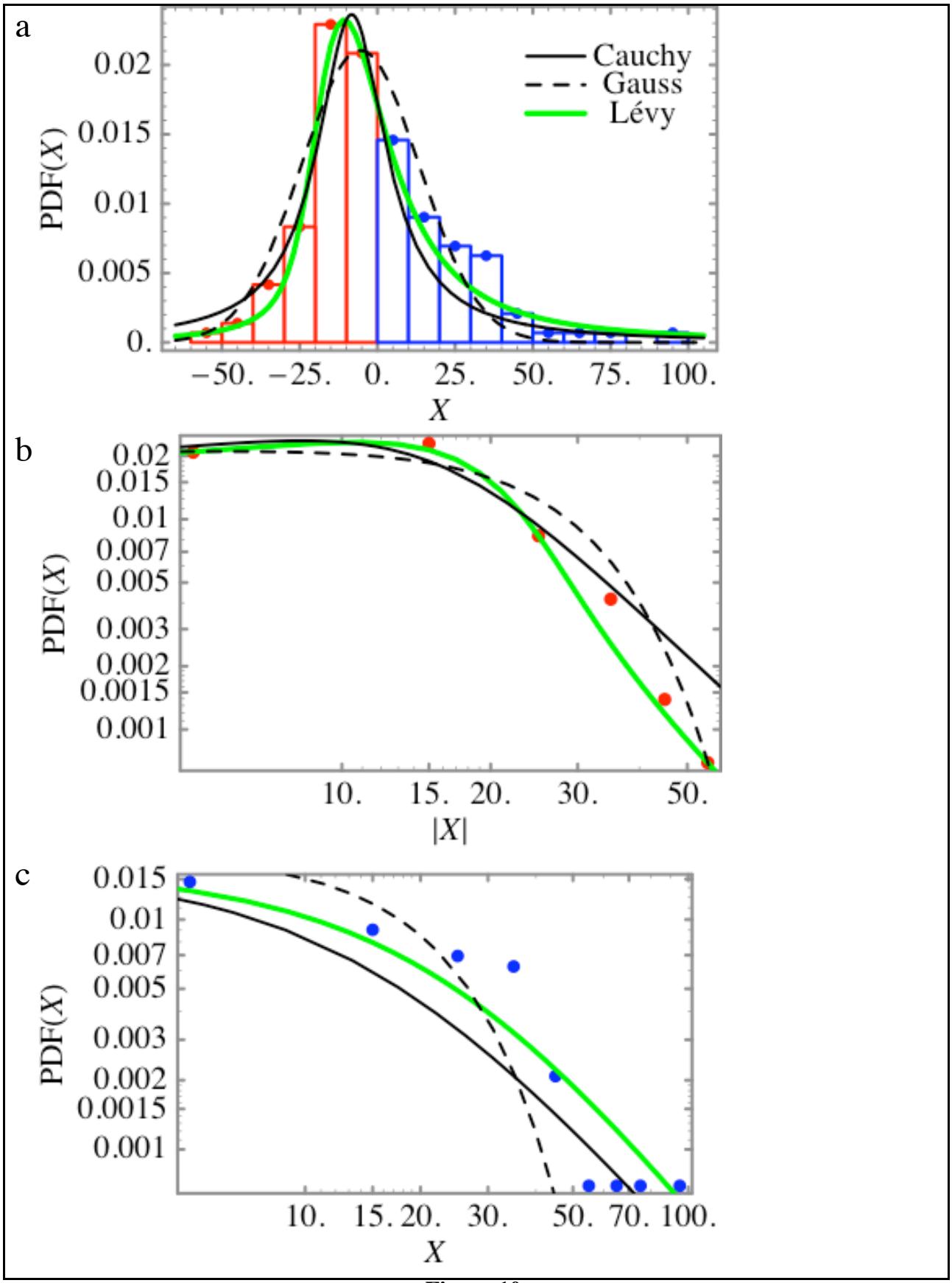
a
0.02
0.015
0.01
0.005
0.
PDF(X)
Cauchy
Gauss
Lévy
−50. −25. 0. 25. 50. 75. 100.
X
b
0.02
0.015
0.01
0.007
0.005
0.003
0.002
0.0015
0.001
PDF(X)
10. 15. 20. 30. 50.
|X|
c
0.015
0.01
0.007
0.005
0.003
0.002
0.0015
0.001
PDF(X)
10. 15. 20. 30. 50. 70. 100.
X

Figure 10:

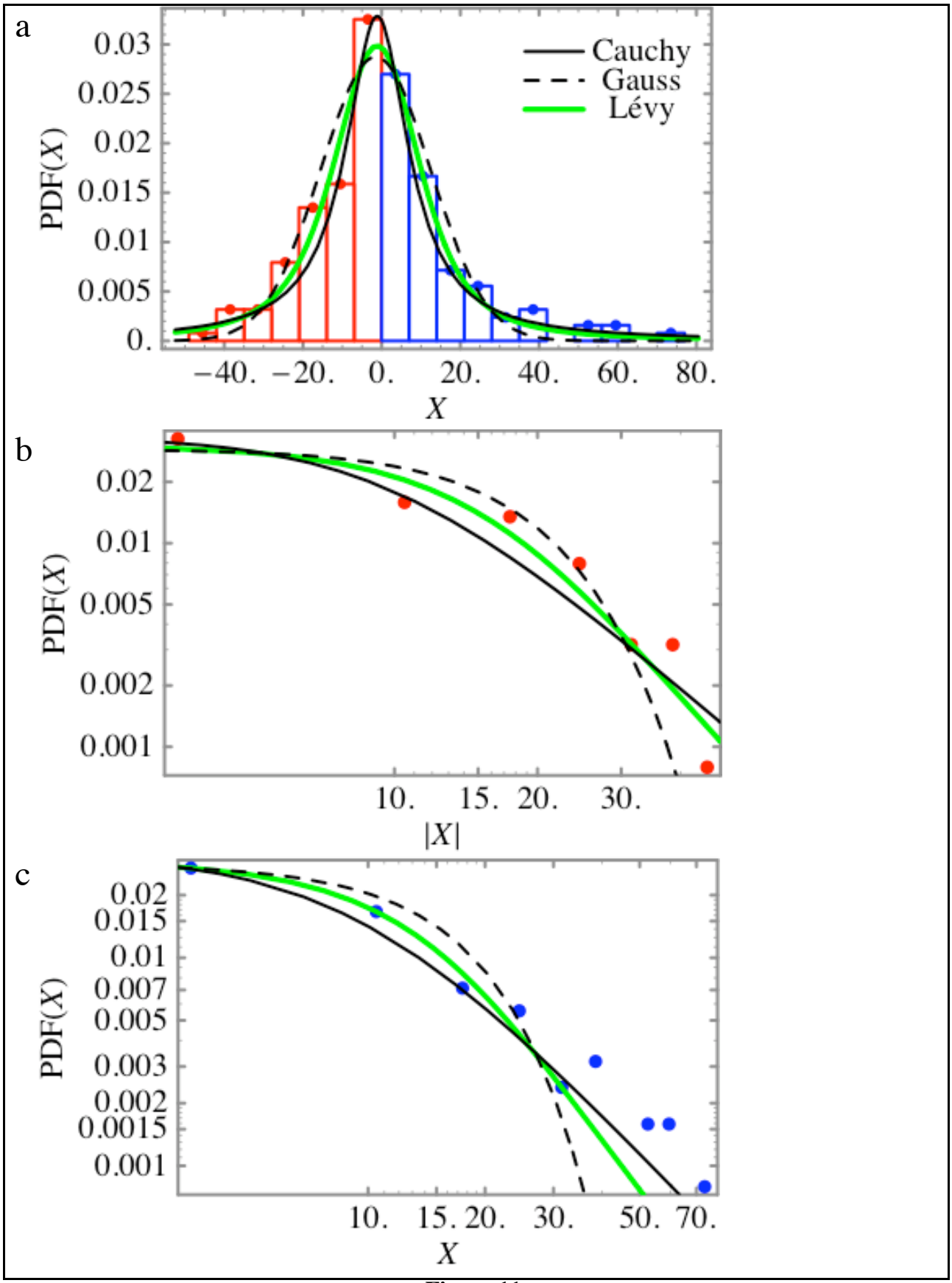
a
0.03
0.025
0.02
0.015
0.01
0.005
0.
PDF(X)
Cauchy
Gauss
Lévy
−40.
−20.
0.
20.
40.
60.
80.
X
b
0.02
0.01
0.005
0.002
0.001
PDF(X)
10.
15.
20.
30.
|X|
c
0.02
0.015
0.01
0.007
0.005
0.003
0.002
0.0015
0.001
PDF(X)
10.
15.
20.
30.
50.
70.
X

Figure 11:

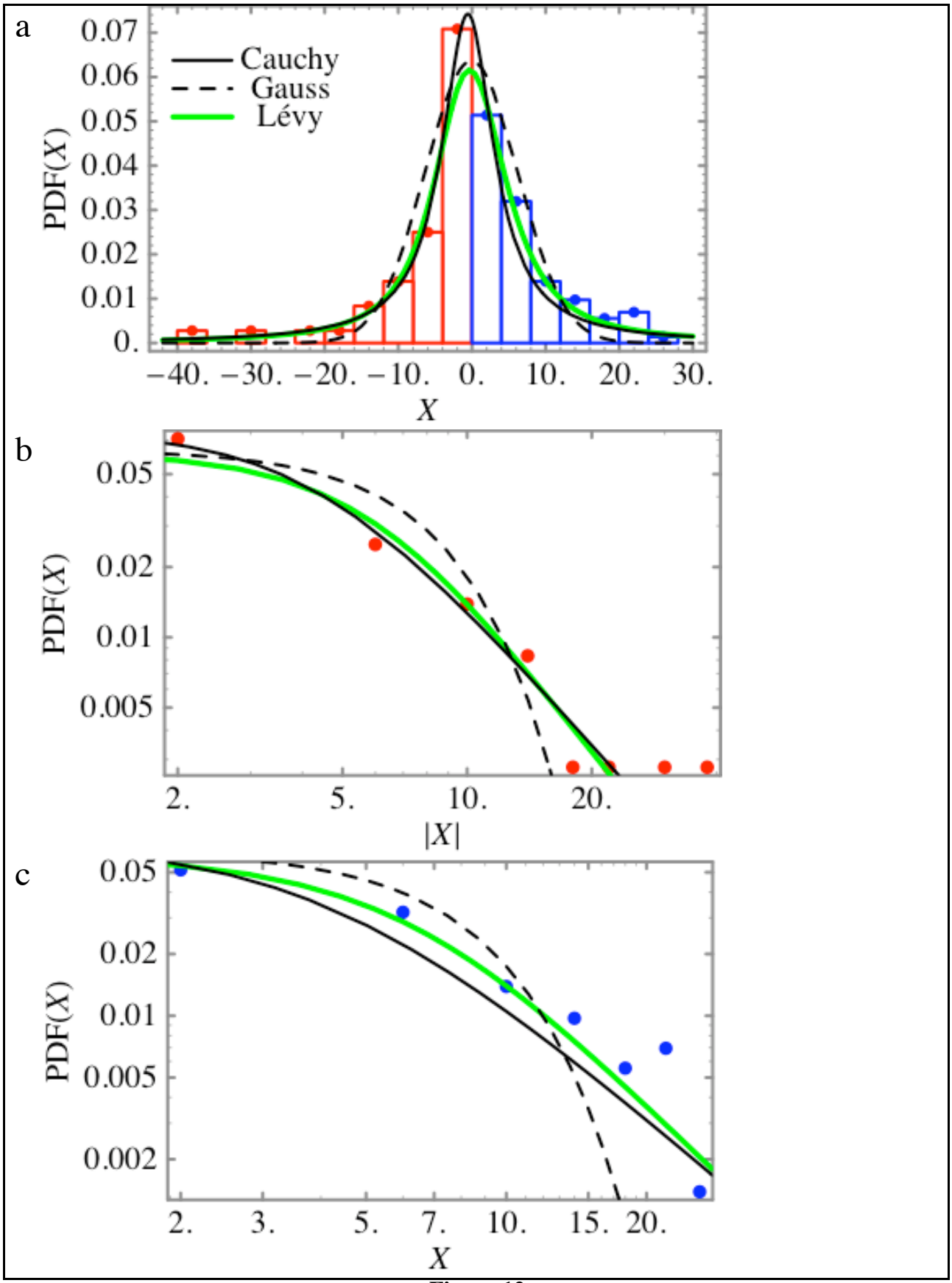
a
0.07
0.06
0.05
0.04
0.03
0.02
0.01
0.
PDF(X)
Cauchy
Gauss
Lévy
−40. −30. −20. −10. 0. 10. 20. 30.
X
b
0.05
0.02
0.01
0.005
PDF(X)
2. 5. 10. 20.
|X|
c
0.05
0.02
0.01
0.005
0.002
PDF(X)
2. 3. 5. 7. 10. 15. 20.
X

Figure 12

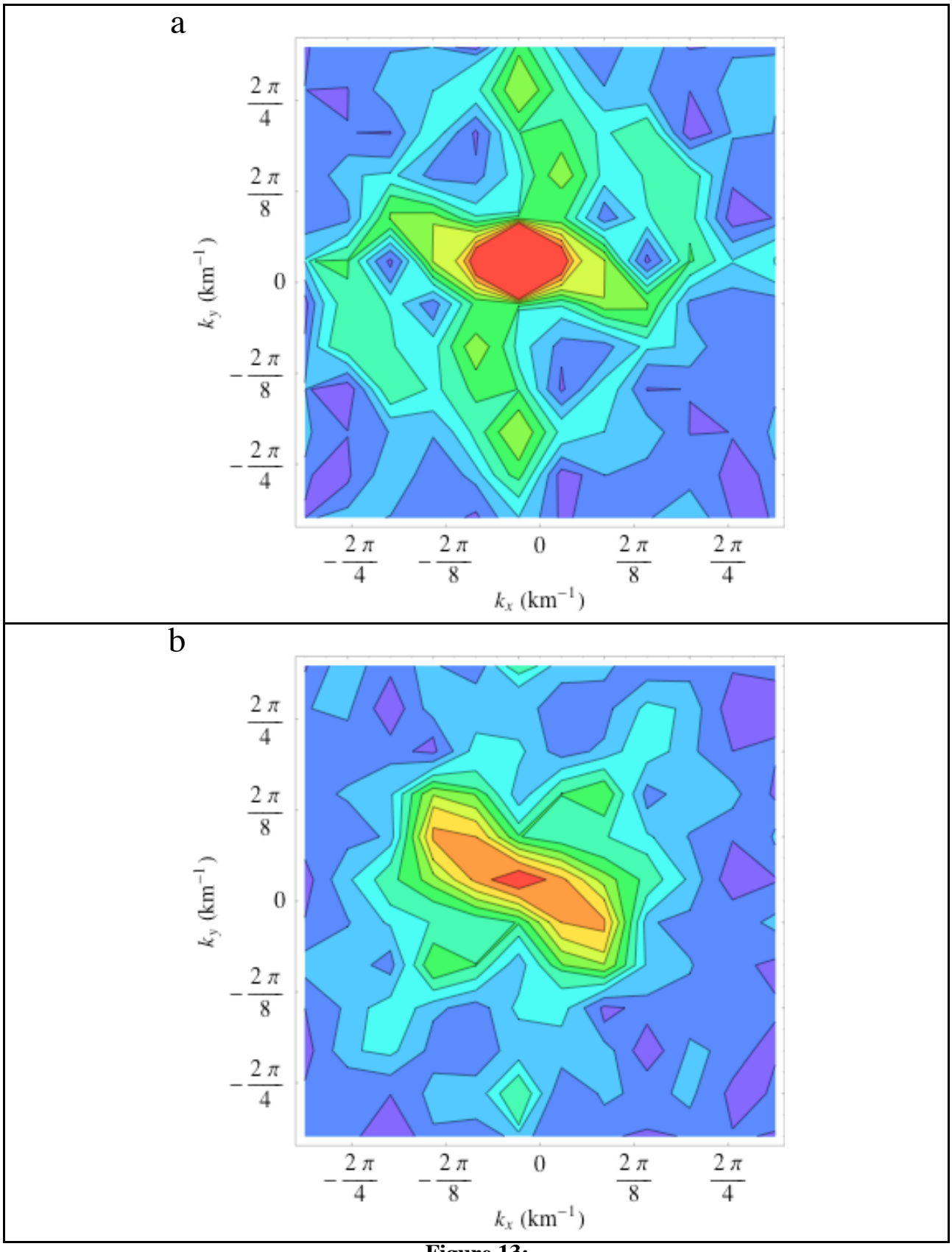
a
$\frac{2\pi}{4}$
$\frac{2\pi}{8}$
0
$-\frac{2\pi}{8}$
$-\frac{2\pi}{4}$
k_y (km^{-1})
$-\frac{2\pi}{4}$
$-\frac{2\pi}{8}$
0
$\frac{2\pi}{8}$
$\frac{2\pi}{4}$
k_x (km^{-1})
b
$\frac{2\pi}{4}$
$\frac{2\pi}{8}$
0
$-\frac{2\pi}{8}$
$-\frac{2\pi}{4}$
k_y (km^{-1})
$-\frac{2\pi}{4}$
$-\frac{2\pi}{8}$
0
$\frac{2\pi}{8}$
$\frac{2\pi}{4}$
k_x (km^{-1})

Figure 13:

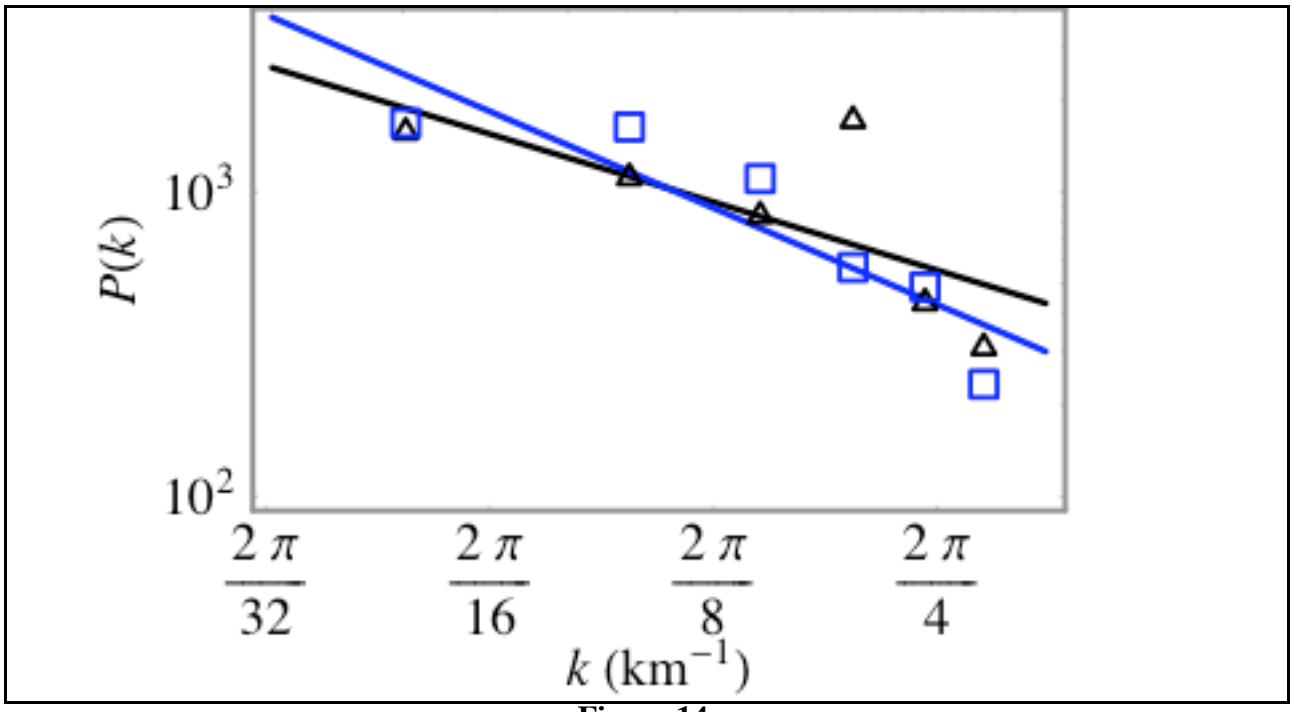

Figure 14:

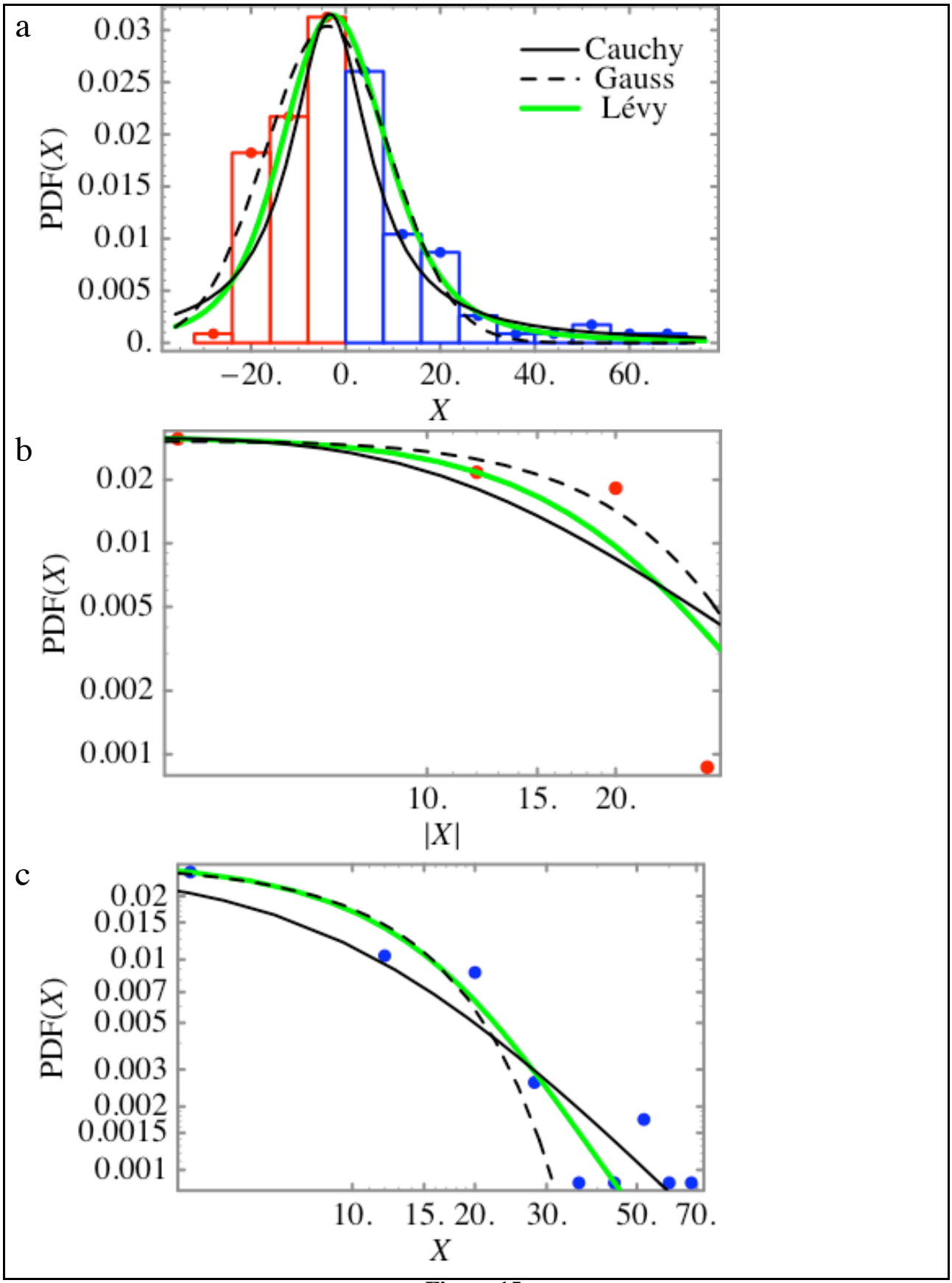
a
0.03
0.025
0.02
0.015
0.01
0.005
0.
PDF(X)
−20.
0.
20.
40.
60.
X
Cauchy
Gauss
Lévy
b
0.02
0.01
0.005
0.002
0.001
PDF(X)
10.
15.
20.
|X|
c
0.02
0.015
0.01
0.007
0.005
0.003
0.002
0.0015
0.001
PDF(X)
10.
15.
20.
30.
50.
70.
X

Figure 15:

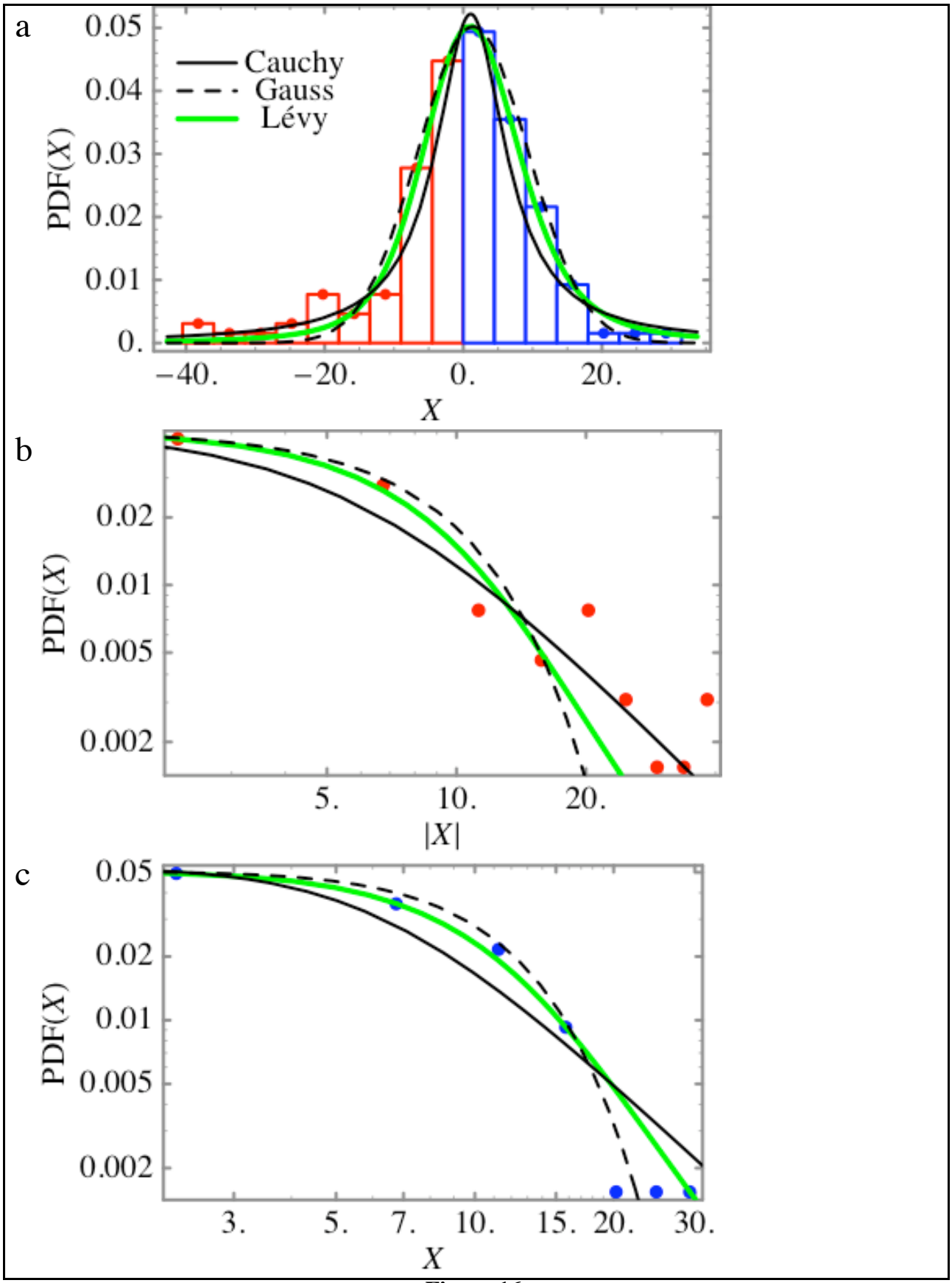
a
0.05
0.04
0.03
0.02
0.01
0.
PDF(X)
Cauchy
Gauss
Lévy
−40.
−20.
0.
20.
X
b
0.02
0.01
0.005
0.002
PDF(X)
5.
10.
20.
|X|
c
0.05
0.02
0.01
0.005
0.002
PDF(X)
3.
5.
7.
10.
15.
20.
30.
X

Figure 16:

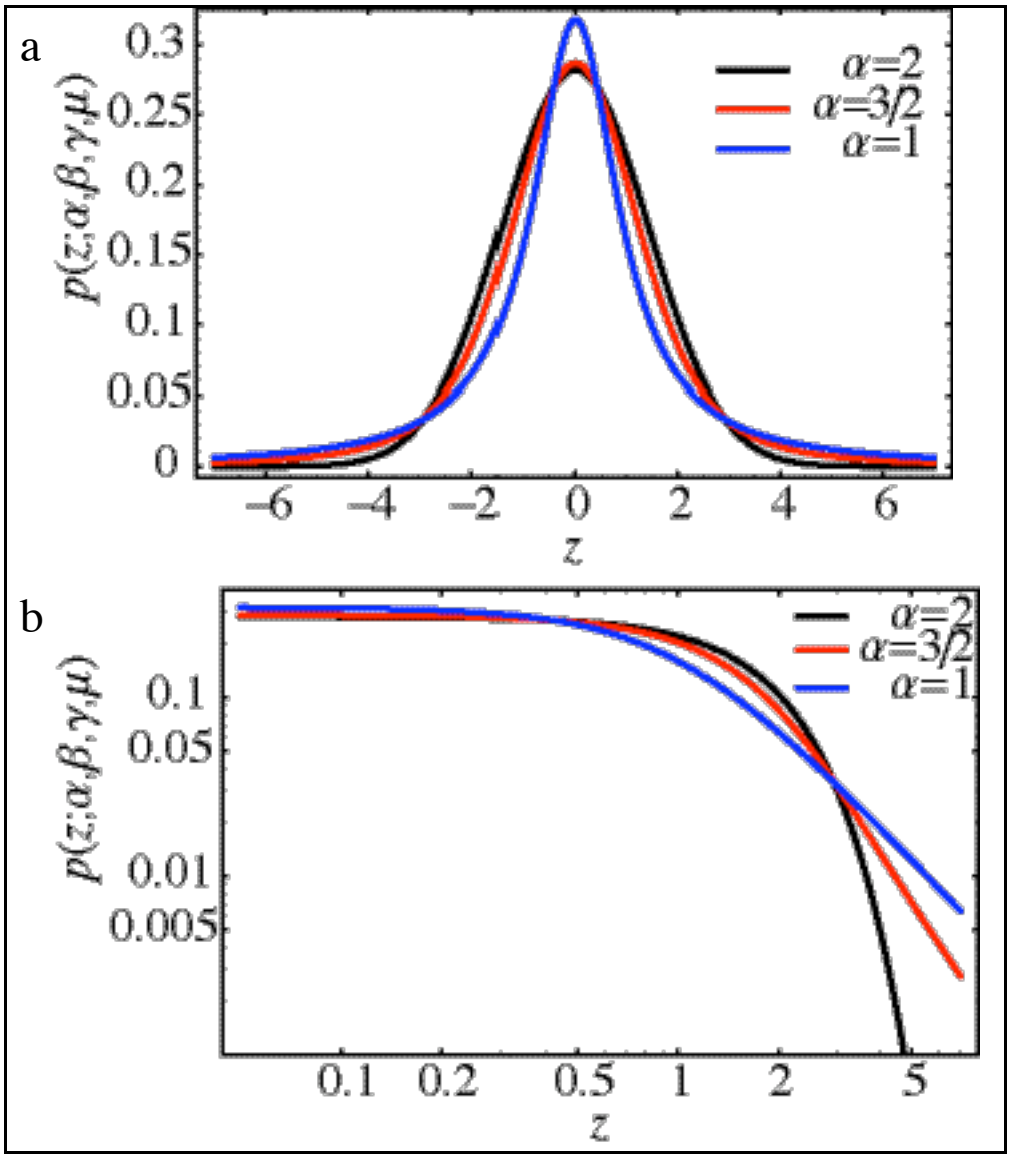
a
0.3
0.25
0.2
0.15
0.1
0.05
0
p(z;α,β,γ,μ)
α=2
α=3/2
α=1
−6
−4
−2
0
2
4
6
z
b
0.1
0.05
0.01
0.005
p(z;α,β,γ,μ)
α=2
α=3/2
α=1
0.1
0.2
0.5
1
2
5
z

Figure A1:

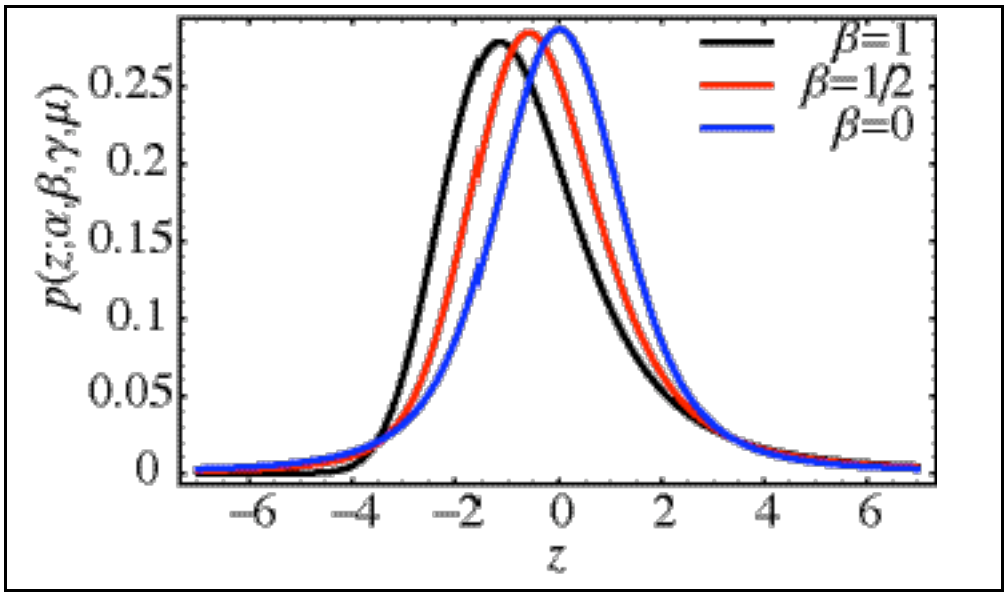

Figure A2:

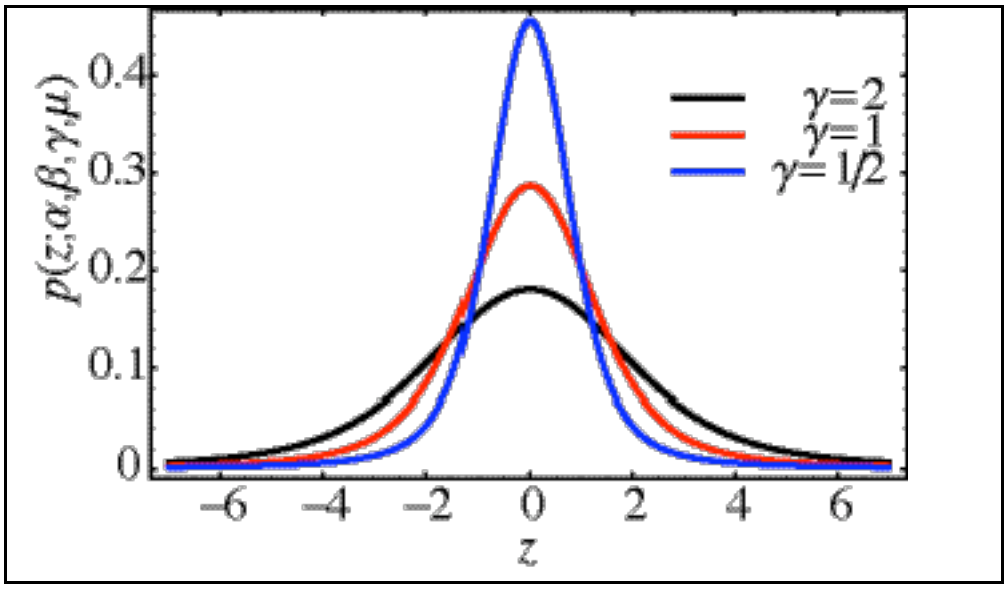

Figure A3:

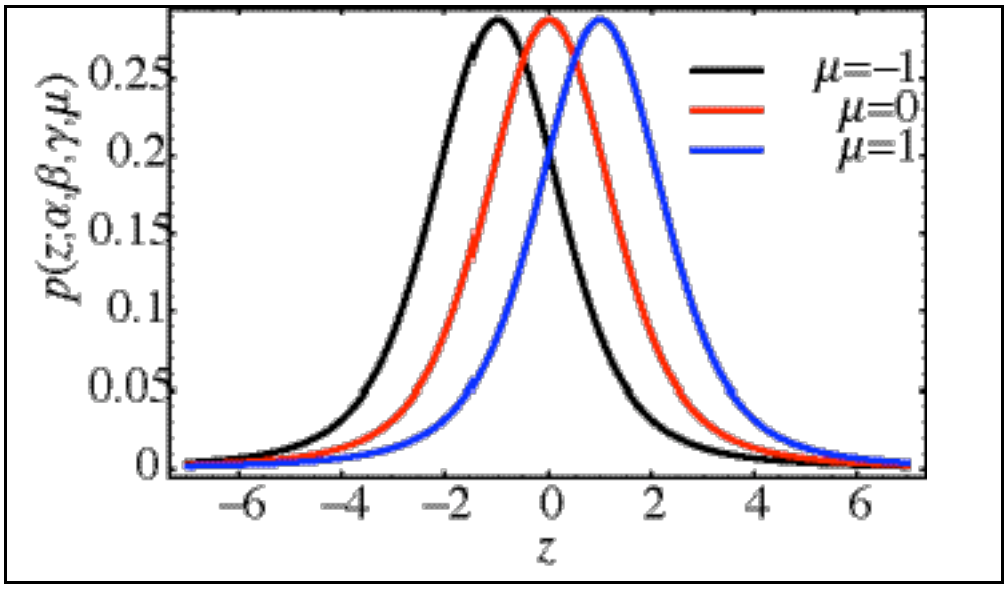

Figure A4:

APPENDIX A: ON THE ESTIMATE (DETERMINATION) OF THE PARAMETERS OF THE LÉVY LAW

In this appendix we discuss the procedure used to estimate the Lévy parameters associated to a set of random variables. We also presents the results obtained when using this procedure on Lévy random variables generated with the proper algorithms. But first we have to introduce the mathematical formulation of the probability density function and characteristic function for the Lévy law (detailed discussions can be found in the literature: Feller, 1971; Grigoriu, 1995; Nikias and Shao, 1995; and Uchaikin and Zolotarev, 1999)

Usually the Lévy probability density function $p(z;\alpha,\beta,\gamma,\mu)$ is given by the Fourier transform of the characteristic function $\varphi(k;\alpha,\beta,\gamma,\mu)$:

$$p(z;\alpha,\beta,\gamma,\mu) = (2\pi)^{-1}\int_{-\infty}^{\infty}\exp(-ikz)\varphi(k;\alpha,\beta,\gamma,\mu)dk \tag{A1}$$

with the functional behavior of the characteristic function given by the following expression:

$$\varphi(k;\alpha,\beta,\gamma,\mu) = \exp[\gamma(ik\mu - |k|^{\alpha} + ik\omega(k;\alpha,\beta))] \tag{A2}$$

and with

$$\omega(k;\alpha,\beta) = \begin{cases} |k|^{\alpha-1}\beta\tan(\alpha\pi/2) \\ -\beta(2/\pi)\ln|k| \end{cases} \tag{A3}$$

The four parameters α, β, γ and μ are limited to a domain of values defined by:

$$0 < \alpha \le 2,\ -1 \le \beta \le 1,\ \gamma > 0, \text{ and } -\infty < \mu < \infty \tag{A4}$$

(see also Section II for a discussion on the parameters; Figures A1 to A4 illustrate the functional behavior of $p(z;\alpha,\beta,\gamma,\mu)$ for different values of the parameters). Note that the representation of the characteristic function is not unique, other forms have been postulated (for a discussion see Uchaikin and Zolotarev, 1999). Traditional literatures on the Lévy law claim that there are only several cases for which the functional behavior of $p(z;\alpha,\beta,\gamma,\mu)$ can be expressed in terms of known

functions. They are the Gauss law for $\alpha = 2$, the Lévy law for $\alpha = 1$ and $\beta = 0$, and the half-normal law (sometime referred as the Lévy law) for $\alpha = 1/2$ and $\beta = 1$. This statement is not accurate anymore since analytical expressions of $p(z;\alpha,\beta,\gamma,\mu)$ have been found for some values of the parameters α, β, γ and μ in terms of generalized hypergeometric functions and Meijer's G functions (see Hoffman-Jorgensen, 1993; Zolatorev, 1995; and Uchaikin and Zolotarev, 1999). Furthermore, using *Mathematica*, it is also possible to compute an analytical expression of the integral in Eq. (A1). For instance for $\alpha = 3/2$ and $\beta = 0$, the following expression is computed:

$$\frac{1}{81\gamma^{2/3}}\left[81\Gamma\left(\frac{5}{3}\right){}_2F_3\left(\frac{5}{12},\frac{11}{12};\frac{1}{3},\frac{1}{2},\frac{5}{6};-\frac{4(z-\mu)^6}{729\gamma^4}\right)+\right.$$
$$7\left(\frac{(z-\mu)^6}{\gamma^4}\right)^{2/3}\Gamma\left(\frac{4}{3}\right){}_2F_3\left(\frac{13}{12},\frac{19}{12};\frac{7}{6},\frac{3}{2},\frac{5}{3};-\frac{4(z-\mu)^6}{729\gamma^4}\right)- \qquad \text{(A5)}$$
$$\left.27\left(\frac{(z-\mu)^6}{\gamma^4}\right)^{3/2}{}_3F_4\left(\frac{3}{4},1,\frac{5}{4};\frac{2}{3},\frac{5}{6},\frac{7}{6},\frac{4}{3};-\frac{4(z-\mu)^6}{729\gamma^4}\right)\right]$$

where ${}_pF_q$ is the generalized hypergeometric function (for details see Gradshteyn and Ryzhik, 1994). However for numerical computation, this analytical representation in term of hypergeometric functions is rather cumbersome and not really useful. First, the analytical form does not exist for all values of the parameters α, β, γ and μ; and when it exists, the integral can be very long to compute as can be the compilation of the hypergeometric functions. For all the results discussed in this paper, the integral in Eq. (A1) was computed numerically using the algorithm NIntegral in *Mathematica*.

In principle, for a given set of discrete values of the probability density function $PDF(X_i)$, one can compute the values of the parameters of the Lévy law that minimize the following expression

$$\sum_{i=1}^{N}\left|PDF(X_i) - p(X_i;\alpha,\beta,\gamma,\mu)\right| \qquad \text{(A6)}$$

under the constraints given in Eq. (A4). In Eq. (A6), X_i is the i^{th} random value and N the number of random variables. For this purpose, we used the optimization algorithm NMinimize provided in

Mathematica. This new optimization algorithm includes several methods for global optimization: genetic programming, nonlinear simplex algorithm and simulated annealing (Wolfram, 2003; additional details are available on the web at http://documents.wolfram.com/v5/Built-inFunctions/NumericalComputation/Optimization/AdvancedDocumentation/NMinimize.html). The expression in Eq. (A6) is computed by using the three methods. Comparing the results obtained by the different methods ensure a better and robust minimization of the expression in Eq. (A6). The results reported in this paper are those corresponding to the method that provides the lowest estimate of Eq. (A6). Also comparing the parameter values through different methods allows the inference of a "margin of error" in the parameter values when such values differ from one method to another. However this procedure is expensive in computer time. This is partially due to the number of parameters to be fit, the constraints in Eq. (A4) and the numerical integration of Eq. (A1). Furthermore, optimization algorithms require initial values for the parameter to be fit. The choice of the initial values also affects the duration of the compilation —and sometimes finding an optimal solution. To achieve a faster computation, and hopefully a more robust compilation of the parameter values, we have devised an iterative procedure allowing a better choice for the initial values to be fed in the algorithm NMinimize.

First it should be noted that as an alternative to optimizing Eq. (A5), one can rather, or additionally, optimize an objective function based on the characteristic function (Grigoriu, 1995 and reference therein):

$$\sum_k \left| \varphi\left(k;\alpha,\beta,\gamma,\mu\right) - \varphi_k \right| \tag{A7}$$

The characteristic function φ_k, associated to the random variables X, is computed by estimating the following expression:

$$\varphi_k = \left\langle Exp(ikX) \right\rangle \tag{A8}$$

where k is the wave number and $\left\langle f \right\rangle$ is the expected (or mean) values of f. The characteristic function φ_k is well located in the wave number space and almost zero outside a finite interval of k values. However, the values of k used to compute φ_k in Eq. (A8) have to be chosen carefully,

especially large values of k since accurate compilation of φ_k is more difficult to achieve as the value of k increases. (Note that these values are independent of the values used in the power spectrum analysis discussed earlier in this paper.) One can also observe that the absolute value of the characteristic function given by Eq. (A2) is only specified by two parameters (see Uchaikin and Zolotarev, 1999):

$$\varphi_A(k;\alpha,\gamma) = \left|\varphi(k;\alpha,\beta,\gamma,\mu)\right| = \exp[-\gamma|k|^\alpha] \tag{A9}$$

and that an objective function associated with $\varphi_A(k;\alpha,\gamma)$ can be computed and optimized to determine the values of the parameters α and γ. The objective function to be optimized is given by the following expression:

$$\sum_k \left| \varphi_A(k;\alpha,\gamma) - |\varphi_k| \right| \tag{A10}$$

The procedure used to estimate the parameters of the Lévy law can be summarized by the following steps:

1- Compute the parameters γ and μ that optimize expression (A6) for a Gauss and a Cauchy law. In this computation, we use the well-known analytical expressions for the Gauss $p(z;2,0,\gamma,\mu)$ and Cauchy $p(z;1,0,\gamma,\mu)$ probability density functions.

2- Compute the parameters α and γ that optimize expression (A10). For this purpose, we use as initial values for α and γ the values obtained in the first step, either the Gauss or Cauchy parameters depending which one provide the lowest value for the objective function in expression (A6).

3- Compute the parameters α, β, γ and μ that optimize expression (A7). We use as α, β, γ and μ initial values the values computed in the second step and the first step.

4- Compute the parameters α, β, γ and μ that optimize expression (A6). We use as initial values for the parameters to be determined those obtained in the third step.

Note that intermediary steps can be added to this procedure. For instance, in steps 3 or 4, one can use the value of α and γ found in the second step and optimize expressions (A6) or/and A7 to only

fit the parameters β and μ. If the computer is too slow, one can consider replacing step 4 by this variation. Note also that to provide robust results, it is better to perform the computation for different sets of initial values of the parameters. This will also ensure (as much as possible) that the optimization compilation is not trapped in a local minimum. For the three last steps, we used the *Mathematica* algorithm NMinimize for all the results presented in this paper, with the three methods for global optimization: genetic programming, nonlinear simplex algorithm and simulated annealing. For the first step, we either use NMinimize or NonlinearRegress.

To assert its soundness, the procedure to compute the Lévy parameters has to be tested. Furthermore, the procedure has to be tested under conditions that are as close as possible to the conditions used to compute the Lévy parameters associated with the slip distribution. For this purpose, we have generated two hundred Lévy random variables using the algorithms discussed in Chambers et al., (1976) —see also Grigoriu (1995)— and Nikias and Shao (1995) with different values for the parameters α, β, γ and μ. (These algorithms should be used carefully, since depending on the seed and the number of random variables generated; convergence toward the theoretical distribution is not automatic.) The number of random variables was chosen to match roughly the number of events (sub-faults) used in the analysis of the slip spatial distributions: 144 (Loma Prieta), 180 (Northridge), 196 (Imperial Valley) and 280 (Hyogo ken Nanbu —Kobe). The probability density function and the characteristic function —see Eq. (A8)— associated with these random variables have been computed. Then the procedure discussed above was used to compute the best-fitting values for the parameters α, β, γ and μ. Comparison between the best-fitting values computed at each iteration and the original values used to generate the random variables are presented in Tables A1 to A7. In Tables A3 and A4, the values of the parameters are identical but the algorithm used to generate the Lévy random variables is different: the algorithm of Chambers et al., (1976) in Table A3 and the algorithm given in Nikias and Shao (1995) in Table A4. These results indicate the order of accuracy that can be expected for the parameters when considering two different samples of two hundred (iid) Lévy random variables.

The tests done using the procedure outlined above allow us to draw some conclusions. In general, the values for the parameters γ and μ, that respectively characterized the dispersion and location of the probability density function, are well estimated in term of their order of magnitude. This conclusion holds independently of the law or method used to estimate the parameters. For most of the studies, the procedure provides accurate values of the parameter α as long as the values of α are not too low. (For a set of two hundred variables, it is more difficult to approximate the theoretical behavior of the probability density function when $\alpha \approx 0.7$ or smaller.) Of all the four parameters, β is the parameter estimated with the least accuracy, although the parity is usually well resolved. The asymmetry or symmetry of the probability density function curves is not well resolved for the number of random variables used in these tests.

The question of how many random variables are needed to get an accurate estimate of the PDF and of the PDF parameters is beyond the scope of this paper. What we want to establish in this Appendix, is that given a number of random variables similar to those used in computing the stochastic model of the slip distribution and using a similar procedure, is it possible to discriminate between a Gaussian ($\alpha = 2$), a Cauchy noise ($\alpha = 1$, $\beta = 0$) and a Lévy noise with a stable parameter value α not too close to 1 or 2? The study suggests that the parameter α can be estimated with an approximation of roughly ±0.3 (see Tables A4 and A5). This precision is for generated (iid) random variables. For random noise obtained through the filtering of the slip distribution, the uncertainty is surely larger although not easily quantified. These results suggest that the uncertainty on the values of the parameter α reported in Tables 1 to 3 is at least of the order of ±0.3. Within this margin of error, it is possible to distinguish between a Cauchy ($\alpha = 1$) and a Gaussian ($\alpha = 2$) random law. For the sake of comparison, with results presented in Tables 1 to 7, we present in Table A8 the results of the procedure outlined above for the dip slip of the Northridge earthquake illustrated in Figure 11.

Finally, the computed values for the parameters of the Cauchy, Gauss and Lévy laws depend to a certain extent on the size of the increment ΔX used to compute the $PDF(X)$. However numerical compilations of the parameters of the Cauchy, Gauss and Lévy laws for a reasonable

choice of ΔX show that there is no significant change in the parameter values. For instance the values presented in Table 8 has been computed for $\Delta X = 7$ (see Figure 11). Using a $\Delta X = 8$ to compute the $PDF(X)$, we obtain that the Gauss law is best fit for $\gamma = 96.14$ and $\mu = -1.55$; the Cauchy law is best fit for $\gamma = 10.35$ and $\mu = -1.72$; and the Lévy law is best fit for $\alpha = 1.28$, $\beta = 0.14$, $\gamma = 18.34$ and $\mu = 0.76$. These values are in good agreement with those reported in Table 8. That is, the results presented in Tables 1 to 3, indicating that the Lévy law provides a better fit, are not an artifact that can be eliminated by choosing another reasonable value for ΔX. By reasonable value of ΔX we mean a value as small as possible —to get as many points as possible to fit the three probability laws— but large enough to reproduce the regular smooth shape associated to a probability density function. There is not optimal way to make such a choice, and it may be possible to get better results by using a variable ΔX. For N random variables X_i we perform the following comparison to insure a reasonable choice of ΔX. First we computed the mean directly from the data, using $(1/N)\sum_{i=1}^{N} X_i$, and compare to the mean computed with $\sum_{i=1}^{N} PDF(X_i)\, X_i$, using the computed $PDF(X)$ at a given ΔX. Than we computed the moment of second order directly from the data, using $(1/N)\sum_{i=1}^{N} X_i^2$, and compared with the moment of second order computed with $\sum_{i=1}^{N} PDF(X_i)\, X_i^2$. The increment ΔX is chosen in such a way that both comparisons give similar values for the mean and the moment of second order.